Study of parameterizations for the rigid body transformations of the scan registration problem

Andreas Nüchter [a,*], Jan Elseberg [a], Peter Schneider [b], Dietrich Paulus [b]

[a] *Jacobs University Bremen, School of Engineering and Science Campus Ring 1, 28759 Bremen, Germany*
[b] *University of Koblenz-Landau, Institute for Computational Visualistics, Active Vision Group, Universitätsstr. 1, 56070 Koblenz, Germany*

ARTICLE INFO

ABSTRACT

The iterative closest point (ICP) algorithm is the de facto standard for geometric alignment of three-dimensional models when an initial relative pose estimate is available. The basis of the algorithm is the minimization of an error function that takes point correspondences into account. Four closed-form solution methods are known for minimizing this function. This paper presents novel linear solutions to the scan registration problem, i.e., to the problem of putting and aligning 3D scans in a common coordinate system. We extend the methods for registering *n*-scans in a global and simultaneous fashion, such that the registration of the *n*th scan influences all previous registrations in *one* step.

© 2010 Elsevier Inc. All rights reserved.

1. Introduction

Registering 3D models, i.e., putting two or more 3D scans in a common coordinate system, is a crucial step in 3D model construction. Many applications use the iterative closest point (ICP) algorithm. Nowadays precise 3D scanners are available that are used in architecture, industrial automation, agriculture, cultural heritage conservation, and facility management. Other applications of point cloud registration algorithms include medical data processing, art history, archaeology, and rescue and inspection robotics. The recent advent of time-of-flight (TOF) 3D cameras is likely to generate another burst of ICP-like applications in the near future [55,51,54].

The ICP algorithm registers two independently acquired 3D scans or 3D point clouds into a common coordinate system. Here the algorithm relies on minimizing an error function over closest point correspondences. The following analogy is often used to depict the minimization issue: the correspondences represent a system of springs that forces the scan to be aligned to the correct position. Four closed-form solution methods are known for minimizing the ICP error function [28]. The difficulty in minimizing the ICP error function is to ensure the orthonormality constraint of the included rotation matrix. This paper presents linearized solution methods, where the optimal rotation is approximated by solving a system of linear equations. The linearization methods are the helix transform, the small angle approximation, and the uncertainty-based registrations. For the latter one we model the

scan pose, i.e., position and orientation, as Gaussian distributions and use the Euler and the quaternion representation. Our objective is to compare different gradient descent algorithms based upon different rotation parameterizations to solve the bundle adjustment problem that arises with 3D point clouds produced by range finders. In [46] the recommendation concerning the parameterization choice is stated as:

> "*Similarly, experience suggests that quasi-global 3 parameter rotation parameterizations such as Euler angles cause numerical problems unless one can be certain to avoid their singularities and regions of uneven coverage. Rotations should be parameterized using either quaternions subject to* $|\dot{q}|^2 = 1$*, or local perturbations* $\mathbf{R}\delta\mathbf{R}$ *or* $\delta\mathbf{R}\mathbf{R}$ *of an existing rotation* $\mathbf{R}$*, where* $\delta\mathbf{R}$ *can be any well-behaved 3 parameter small rotation approximation, e.g.,* $\delta\mathbf{R} = (\mathbf{I}_{3\times3} + [\delta\mathbf{r}]_\times)$*, the Rodriguez formula, local Euler angles, etc.*".

Recently, Grisetti et al. [21] used a gradient descent technique for 3D robotic mapping incorporating incremental spherical linear interpolation [2]. Also Mitra et al. [31] and Hertzberg [22] make use of some gradient descent method for registration. This paper focuses on the issue of linearization of the rotation manifold and studies alternative methods.

If *n*-scans have to be registered, any sequential application of ICP will accumulate errors, and therefore the ICP algorithm has to be extended. Fig. 1 presents an urban scene digitalized with roughly 1000 3D scans. The accompanying video demonstrates the ICP scan matching and the loop closing, when the robot that acquires the 3D scans returns to a location where it has been before. Every frame corresponds to an ICP scan matching (we skip the animation of the actual ICP scan matching), or to one

---

* Corresponding author.
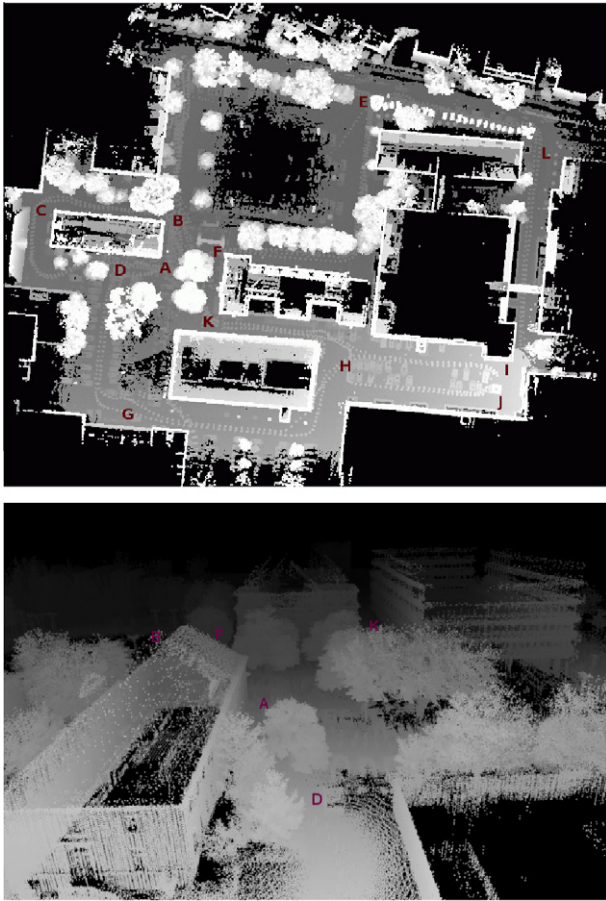 *E-mail address:* andreas@nuechti.de (A. Nüchter).

Fig. 1. Registration of *n*-scans. Top: scene HANNOVER2 of an urban environment in a bird's eye view. The scans have been taken according to the trajectory: A-B-C-D-A-B-E-F-A-D-G-H-I-J-H-K-F-E-L-I-K-A. A video of the scan matching process can be found under http://www.plum.eecs.jacobs-university.de/submissions/large_slam.mpg. Bottom: 3D view of the scene viewed from the left side.

step of the global scan matching (red frames). Locally consistent registration algorithms retain the analogy of the spring system [12] and the resulting algorithms need many iterations for minimizing the global error function. However, globally consistent algorithms minimize the error function in one step. Therefore, it is more likely to reach the global and hopefully the correct optimum. Fig. 2 shows the accumulated error when performing sequential ICP scan matching and the result of globally consistent scan matching. Fig. 3 stresses the difference between global and local optimal results and gives a schematic illustration of the difference.

This paper presents linear solutions to the global *n*-scan registration problem. The two-scan cases are extended to *n*-scans, thus a system of linear equations is built and finally solved to yield new scan poses. The presented methods are examined with respect to computational requirements and to approximation and implementation issues.

The paper is structured as follows: next we summarize the state of the art for 3D registration of laser scans. Since this technique is often used in robotics for mapping, we will also briefly discuss current developments in this field. Then we present the two-scan registration methods. Section 4 presents the solutions to the *n*-scan registration problem followed by a detailed analysis. Finally, Section 6 presents the experiments and results. Inspired by these evaluations we develop an additional solution to the *n*-scan registration problem in Section 7, which turns out to subsume an already given solution. Finally, Section 8 concludes.

2. State of the art

2.1. The ICP algorithm

The following method is the de facto standard for registration of point sets. The complete algorithm was invented at the same time in 1991 by Besl and McKay [5], by Chen and Medioni [10] and by Zhang [50]. The method is called the iterative closest point (ICP) algorithm.

Given two independently acquired sets of 3D points, $\widehat{M}$ (model set) and $\widehat{D}$ (data set) which correspond to a single shape, we want to find the transformation $(\mathbf{R}, \mathbf{t})$ consisting of a rotation matrix $\mathbf{R}$ and a translation vector $\mathbf{t}$ which minimizes the following cost function:

$$E(\mathbf{R}, \mathbf{t}) = \frac{1}{N} \sum_{i=1}^{N} \|\mathbf{m}_i - (\mathbf{R}\mathbf{d}_i + \mathbf{t})\|^2, \tag{1}$$

All corresponding points can be represented in a tuple $(\mathbf{m}_i, \mathbf{d}_i)$, where $\mathbf{m}_i \in M \subset \widehat{M}$ and $\mathbf{d}_i \in D \subset \widehat{D}$. Two things have to be calculated: first, the corresponding points, and second, the transformation $(\mathbf{R}, \mathbf{t})$ that minimizes $E(\mathbf{R}, \mathbf{t})$ on the basis of the corresponding points. The ICP algorithm uses closest points as corresponding points. A sufficiently good starting guess enables the ICP algorithm to converge to the correct minimum.

Current research in the context of ICP algorithms mainly focuses on fast variants of ICP algorithms [39]. If the input are 3D meshes then a point-to-plane metric can be used instead of Eq. (1). Minimizing using a point-to-plane metric outperforms the standard point-to-point one, but requires the computation of normals and meshes in a pre-processing step.

The computation of closest points is the most expensive step in the ICP algorithm. Using the optimized *k*-d trees the cost for finding the closest point to a given query point is at average in the order of $O(\log N)$ [19], thus the overall cost is $O(N \log N)$ (expected time). *Note: N* can be very large; advanced high-precise 3D laser scanners such as the Zoller + Fröhlich yield a data rate up to 500,000 3D points per second [53]. Improvements to *k*-d tree search have been presented. They include approximate *k*-d tree search [20], registration using *d*2-trees [31] and cached *k*-d tree search [32].

2.2. Marker and feature-based registration

To avoid issues with starting guess in the ICP framework, marker based registration uses defined artificial or natural landmarks as corresponding points. This manual data association ensures that by minimizing Eq. (1) the scans are registered at the correct location. Iterations are no longer required. Feature based algorithms, like using SIFT features, automatically extract the 3D position of natural features and do not need any iterations nor manual interference for registration [7].

While registering several 3D data sets using the ICP algorithm or marker and feature-based registration techniques, errors sum up. These errors are due to imprecise measurements and small registration errors. Therefore, globally consistent scan matching algorithm aim at reducing these errors.

2.3. Globally consistent scan matching

Chen and Medioni [11] aimed at globally consistent range image alignment when introducing an incremental matching method, i.e., all new scans are registered against the so-called metascan, which is the union of the previously acquired and registered scans. This method does not spread out the error and is order-dependent.

Bergevin et al. [4], Stoddart and Hilton [41], Benjemaa and Schmitt [2,3], and Pulli [38] present iterative approaches. Based
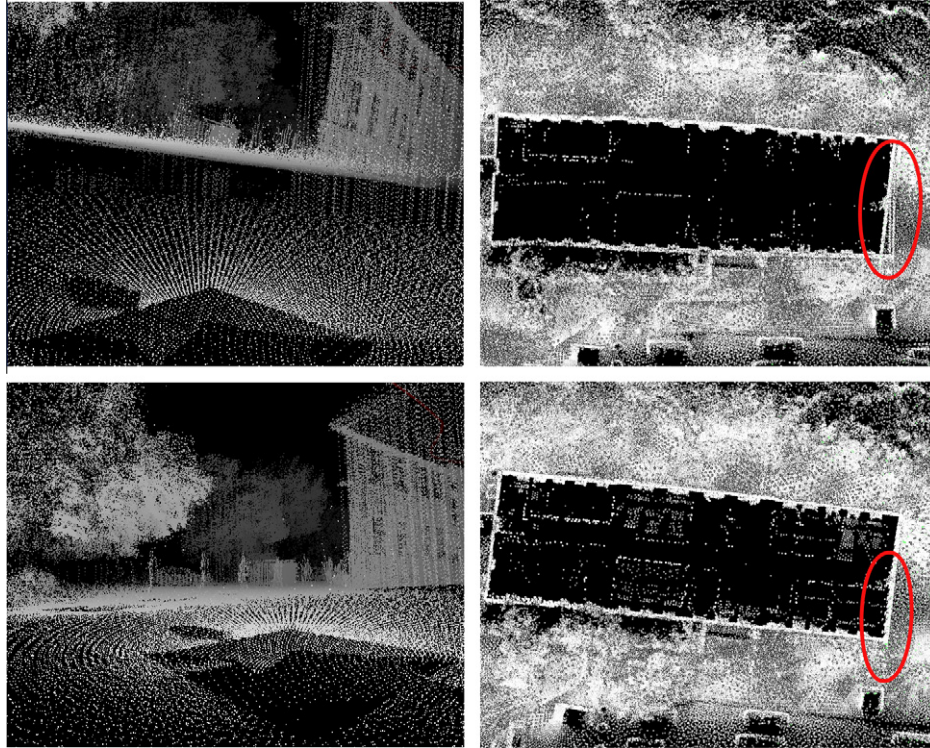
Fig. 2. Top left: 3D view of the scene with the accumulated error during the sequence A-B-C-D-A, where we recorded 135 3D scans. Top right: Scene in a bird's eye view. Bottom row: Consistent registration results. Left: Globally consistent registration in 3D view. Right: Bird's eye view.
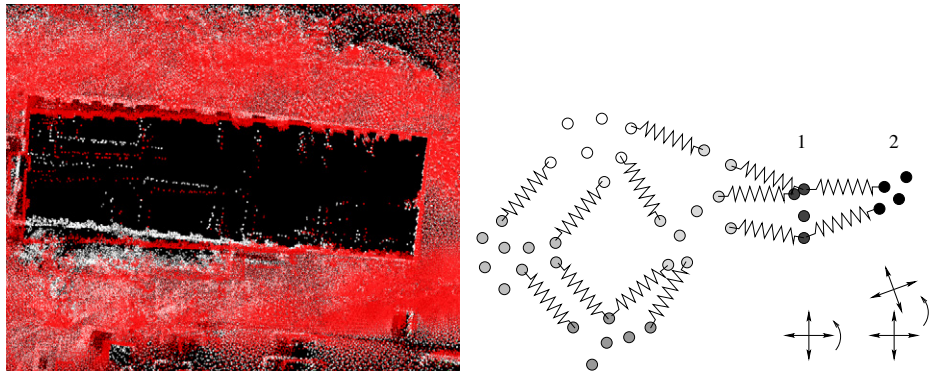

Fig. 3. Left: Locally consistent algorithms reduce the registration errors at the loop closing point but fail to distribute the error. Here in comparison with the global optimal result in bird's eye view (cf. Fig. 2). Right: Schematic view of the registration of 6 scans, whose points are represented by different gray values. Algorithms working locally optimal move every scan separately, while global optimal algorithms minimize all distances at the same time. This includes especially, that the transformation of scan 1 is continued to scan 2 (the rightmost one), i.e., incorporating a "leverage effect".

on networks representing overlapping parts of images, they use the ICP algorithm for computing transformations that are applied after all correspondences between all views have been found. However, the focus of research is mainly 3D modeling of small objects using a stationary 3D scanner and a turn table; therefore, the used networks consist mainly of one loop [38], where the loop closing has to be smoothed. These solutions are locally consistent algorithms that stick to the mentioned analogy of the spring system [12] whereas true globally consistent algorithms minimize the error function in one step.

A probabilistic approach was proposed by Williams et al. [48], where each scan point is assigned a Gaussian distribution in order to model the statistical errors made by laser scanners. This causes high computation time due to the large amount of data in practice. Krishnan et al. [27] presented a global registration algorithm that

minimizes the global error function by optimization on the manifold of 3D rotation matrices.

2.4. Current trends

Recently, alternatives to ICP has been presented. Registration without ICP was described by Pottmann et al. [37] by relying on the geometry of the squared distance function of a scanned surface. In addition, the normal distribution transform (NDT) was proposed as an alternative to the ICP algorithm [6,30]. The NDT divides the 3D space into boxes and correlates all boxes of two scans, yielding more reliable scan matching with respect to the starting guess compared to the ICP algorithm at the expense of computational costs. An extension to the NDT algorithm to globally consistent scan matching is still missing.

2.5. Robotic 3D mapping

Simultaneous Localization and Mapping (SLAM) is the problem of building a map of an unknown environment with a mobile robot while at the same time navigating in the environment, using the unfinished map. The map building problem is a fundamental problem in robotics, since the presence of an accurate map is needed in many applications. The development of solutions to the localization problem as well as the SLAM problem exploit probabilistic methods[42], resulting in a de facto standard, i.e., probabilistic robotics [44]. States of the robot and its environment are represented by probability distributions and the application of Bayes rule allows to integrate sensor measurements. Depending on the representation of the probability distributions we see Kalman filters (Gaussians) [15], grid based approaches (non-Gaussians)[43], and particle filters (sample based non-Gaussians) [45]. The latter two approaches keep for one state several hypothesis at the time. Thus, they are computationally more expensive, but add reliability to the robotic system.

Progress in sensing technology and the need to handle more degree of freedom, resulted in a step backwards and one-hypothesis systems are again set-up. However, probabilistic representations are still preferred, e.g., in [16,14,33,21].

3. 2-Scan registration

Four algorithms are currently known that solve the error function of the ICP algorithm in closed form [28]. These algorithms are briefly discussed next, followed by the description of our linear solutions.

3.1. Closed-form solutions

Four algorithms are currently known that solve the error function of the ICP algorithm in closed form [28]. The difficulty of this minimization is to enforce the orthonormality constraint for the rotation matrix $\mathbf{R}$. Three of these algorithms separate the computation of the rotation $\mathbf{R}$ from the computation of the translation $\mathbf{t}$. These algorithms compute the rotation first and afterward the translation is derived using the rotation. For this separation, two point sets M' and D' have to be computed, by subtracting the mean of the points that are used in the matching:

$$\mathbf{c}_m = \frac{1}{N}\sum_{i=1}^{N}\mathbf{m}_i, \quad \mathbf{c}_d = \frac{1}{N}\sum_{i=1}^{N}\mathbf{d}_i \qquad (2)$$

and

$$M' = \{\mathbf{m}_i' = \mathbf{m}_i - \mathbf{c}_m\}_{1,\dots,N}, \quad D' = \{\mathbf{d}_i' = \mathbf{d}_i - \mathbf{c}_d\}_{1,\dots,N}. \qquad (3)$$

After replacing Eq. (2) and (3) in the error function, $E(\mathbf{R},\mathbf{t})$ Eq. (1) becomes:

$$E(\mathbf{R},\mathbf{t}) = \frac{1}{N}\sum_{i=1}^{N}\|\mathbf{m}_i' - \mathbf{R}\mathbf{d}_i' - \underbrace{(\mathbf{t} - \mathbf{c}_m + \mathbf{R}\mathbf{c}_d)}_{=\tilde{\mathbf{t}}}\|^2$$
$$= \frac{1}{N}\sum_{i=1}^{N}\|\mathbf{m}_i' - \mathbf{R}\mathbf{d}_i'\|^2 - \frac{2}{N}\tilde{\mathbf{t}}\cdot\sum_{i=1}^{N}(\mathbf{m}_i' - \mathbf{R}\mathbf{d}_i') + \frac{1}{N}\sum_{i=1}^{N}\|\tilde{\mathbf{t}}\|^2. \qquad (4)$$

In order to minimize the sum above, all terms have to be minimized. The second sum is zero, since all values refer to centroid. The third part has its minimum for $\tilde{\mathbf{t}} = 0$ or

$$\mathbf{t} = \mathbf{c}_m - \mathbf{R}\mathbf{c}_d.$$

Therefore the algorithm has to minimize only the first term, and the error function is expressed in terms of the rotation only:

$$E(\mathbf{R},\mathbf{t}) \propto \sum_{i=1}^{N}\|\mathbf{m}_i' - \mathbf{R}\mathbf{d}_i'\|^2. \qquad (5)$$

(1) The first method was developed 1987 by Arun, Huang and Blostein [1]. The rotation $\mathbf{R}$ is represented as an orthonormal 3×3 matrix. The optimal rotation is calculated by $\mathbf{R} = \mathbf{V}\mathbf{U}^T$. Here the matrices $\mathbf{V}$ and $\mathbf{U}$ are derived by the singular value decomposition $\mathbf{H} = \mathbf{U}\mathbf{\Lambda}\mathbf{V}^T$ of a cross-correlation matrix $\mathbf{H}$. This 3×3 matrix $\mathbf{H}$ is given by

$$\mathbf{H} = \sum_{i=1}^{N}\mathbf{m}_i'^T\mathbf{d}_i' = \begin{pmatrix} S_{xx} & S_{xy} & S_{xz} \\ S_{yx} & S_{yy} & S_{yz} \\ S_{zx} & S_{zy} & S_{zz} \end{pmatrix}, \qquad (6)$$

where $S_{xx} = \sum_{i=1}^{N} m_{x,i}'d_{x,i}'$, $S_{xy} = \sum_{i=1}^{N} m_{x,i}'d_{y,i}'$, ….

(2) The second method is similar to the previous method and was independently developed in 1988 by Horn, Hilden and Negahdaripour [26]. Again, a correlation Matrix $\mathbf{H}$ according to Eq. (6) is calculated. Afterward a so-called polar decomposition is computed, i.e., $\mathbf{H} = \mathbf{P}\mathbf{S}$, where $\mathbf{S} = (\mathbf{H}^T\mathbf{H})^{1/2}$. For this polar decomposition Horn et al. define a square root of a matrix [26]. Let $\mathbf{H}$, $\mathbf{S}$ and $\mathbf{P}$ the matrices as described above. Then the optimal rotation is given by

$$\mathbf{R} = \mathbf{P} = \mathbf{H}\left(\frac{1}{\sqrt{\lambda_1}}\mathbf{u}_1\mathbf{u}_1^T + \frac{1}{\sqrt{\lambda_2}}\mathbf{u}_2\mathbf{u}_2^T + \frac{1}{\sqrt{\lambda_3}}\mathbf{u}_3\mathbf{u}_3^T\right),$$

where $\{\lambda_i\}$ are the eigenvalues and $\{\mathbf{u}_i\}$ the corresponding eigenvectors of the matrix $\mathbf{H}^T\mathbf{H}$ [26].

(3) The third method finds the transformation for the ICP algorithm by using unit quaternions. This method was invented in 1987 by Horn [25]. The rotation represented as unit quaternion $\dot{\mathbf{q}}$, that minimizes (1), corresponds to the largest eigenvalue of the cross-covariance matrix $\mathbf{N}$

$$\begin{pmatrix} (S_{xx}+S_{yy}+S_{zz}) & (S_{yz}+S_{zy}) & (S_{zx}+S_{xz}) & (S_{xy}+S_{yx}) \\ (S_{yz}+S_{zy}) & (S_{xx}-S_{yy}-S_{zz}) & (S_{xy}+S_{yx}) & (S_{zx}+S_{xz}) \\ (S_{zx}+S_{xz}) & (S_{xy}+S_{yx}) & (-S_{xx}+S_{yy}-S_{zz}) & (S_{yz}+S_{zy}) \\ (S_{xy}+S_{yx}) & (S_{yz}+S_{zy}) & (S_{zx}+S_{xz}) & (-S_{xx}-S_{yy}+S_{zz}) \end{pmatrix}.$$

(4) The fourth solution method for minimizing Eq. (1) uses so-called dual quaternions. This method was developed by Walker, Shao and Volz in 1991 [47]. Unlike the first three methods covered so far the transformation is found in a single step. There is no need to apply the trick with centroids to compute the rotation in a separate fashion. Here, the optimal transformation consisting of a rotation and translation is again a solution of the eigenvalue problem of a 4×4 matrix function that is built from corresponding point pairs.

3.2. Linearized solutions

The closed-form solutions discussed so far are all non-linear, since they need an eigenvector/eigenvalue solver, e.g., in case of using the third method, a quartic equation must be solved [25]. Next, we present four linear solutions for minimizing the ICP error function Eq. (1). The advantage of these linear solutions is that they can be extended straightforward to n-scan registrations.

3.2.1. Registration using the helix transform

Under the assumption that the transformation $(\mathbf{R},\mathbf{t})$ that has to be calculated by the ICP algorithm is small, we can approximate the solution by applying instantaneous kinematics. This solution was initially given by Hofer and Pottmann [24,36] and is repeated here, to make the paper self-contained and to enable us to extend the solution in [24] to the global optimal case.

Instantaneous kinematics computes the displacement of a 3D point by an affine transformation via a so-called helical motion

[36]. A 3D point $\mathbf{p}$ is mapped by adding a small displacement $\mathbf{v}(\mathbf{p})$ given by the parameters $\bar{\mathbf{x}}$ and $\mathbf{x}$, i.e.,

$$\mathbf{v}(\mathbf{p}) = \bar{\mathbf{x}} + \mathbf{x} \times \mathbf{p}.$$

To minimize the ICP error function Eq. (1) the displacement of the points in D has to minimize the distances between the point pairs. Thus Eq. (1) is rewritten as follows:

$$E(\bar{\mathbf{x}}, \mathbf{x}) = \sum_{i=1}^{N} \|\mathbf{m}_i - (\mathbf{d}_i + \mathbf{v}(\mathbf{d}_i))\|^2$$

$$= \sum_{i=1}^{N} \|\mathbf{m}_i - (\mathbf{d}_i + \bar{\mathbf{x}} + \mathbf{x} \times \mathbf{d}_i)\|^2 \tag{7}$$

Since Eq. (7) is a quadratic function with the two unknown variables $\bar{\mathbf{x}}, \mathbf{x}$, the optimal displacement to Eq. (7) is given by the solution of the following linear system: $\bar{\mathbf{x}} + \mathbf{x} \times \mathbf{d}_i = \mathbf{D}_i \cdot \mathbf{u}$, where $\mathbf{u} = (\mathbf{x}^T, \bar{\mathbf{x}}^T)^T$ and

$$\mathbf{D}_i = \begin{pmatrix} 0 & d_{z,i} & -d_{y,i} & 1 & 0 & 0 \\ -d_{z,i} & 0 & d_{x,i} & 0 & 1 & 0 \\ d_{y,i} & -d_{x,i} & 0 & 0 & 0 & 1 \end{pmatrix}$$

$$\sum_{i=1}^{N} \mathbf{D}_i^T \mathbf{D}_i \mathbf{u} = \sum_{i=1}^{N} \mathbf{D}_i^T (\mathbf{m}_i - \mathbf{d}_i) \tag{8}$$

The optimal displacement calculated by Eq. (8) corresponds to an affine motion. Fig. 4 presents the displacement of a point using the affine transformation and rigid transformation. Therefore in a post processing step a rigid transformation $(\mathbf{R}, \mathbf{t})$ is calculated from $(\bar{\mathbf{x}}, \mathbf{x})$ as follows: if $\mathbf{x} = 0$ only a translation is present. In this case $\mathbf{t} = \bar{\mathbf{x}}$ holds. Otherwise an axis G consisting of a direction vector $\mathbf{g}$ and a momentum vector $\bar{\mathbf{g}}$ can be computed. The tuple $(\mathbf{g}, \bar{\mathbf{g}})$ are the Plücker coordinates of the axis G:

$$\mathbf{g} = \frac{\mathbf{x}}{\|\mathbf{x}\|}, \quad \bar{\mathbf{g}} = \frac{\bar{\mathbf{x}} - p\mathbf{x}}{\|\mathbf{x}\|}, \quad p = \frac{\mathbf{x}^T \cdot \bar{\mathbf{x}}}{\mathbf{x}^2}$$

Based on G the point $\mathbf{d}_i$ has to be transformed as follows:

$$\mathbf{d}_i' = \mathbf{R}(\mathbf{d}_i - \mathbf{r}) + (p \; \phi)\mathbf{g} + \mathbf{r} \tag{9}$$

Here $\mathbf{R}$ is the rotation matrix

$$\mathbf{R} = \frac{1}{b_0^2 + b_1^2 + b_2^2 + b_3^2}$$
$$\begin{pmatrix} b_0^2 + b_1^2 - b_2^2 - b_3^2 & 2(b_1 b_2 + b_0 b_3) & 2(b_1 b_3 - b_0 b_2) \\ 2(b_1 b_2 - b_0 b_3) & b_0^2 - b_1^2 + b_2^2 - b_3^2 & 2(b_2 b_3 + b_0 b_1) \\ 2(b_1 b_3 + b_0 b_2) & 2(b_2 b_3 - b_0 b_1) & b_0^2 - b_1^2 - b_2^2 + b_3^2 \end{pmatrix}, \tag{10}$$

where $b_0 = \cos(\phi/2)$, $b_1 = g_x \sin(\phi/2)$, $b_2 = g_y \sin(\phi/2)$, and $b_3 = g_z \sin(\phi/2)$. $\mathbf{g} = (g_x, g_y, g_z)$ is the above mentioned direction vector of the axis G. Furthermore in Eq. (9) $\mathbf{r}$ is an arbitrary point on the axis G. Note: Eq. (10) is similar to the term for computing a rotation matrix from a unit quaternion. Please refer to [24] for more details.
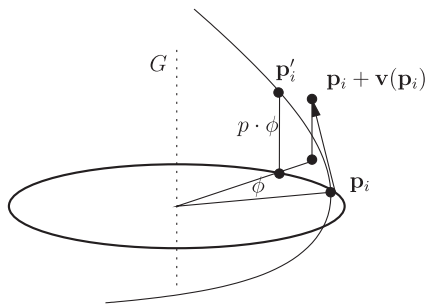

Fig. 4. The affine position of a 3D point $\mathbf{p}_i + \mathbf{v}(\mathbf{p}_i)$ is different from the rigid transformation that results in point $\mathbf{p}_i'$. Based on [24].

3.2.2. Small angle approximation

Next, we develop a novel method based on the small angle approximation. Its basis is again the assumption that the transformation $(\mathbf{R}, \mathbf{t})$ to be calculated by the ICP algorithm is small. Given a rotation matrix $\mathbf{R}$ based on the Euler angles

$$\begin{pmatrix} \cos\theta_y \cos\theta_z & -\cos\theta_y \sin\theta_z & \sin\theta_y \\ \cos\theta_z \sin\theta_x \sin\theta_y + \cos\theta_x \sin\theta_z & \cos\theta_x \cos\theta_z - \sin\theta_x \sin\theta_y \sin\theta_z & -\cos\theta_y \sin\theta_x \\ \sin\theta_x \sin\theta_z - \cos\theta_x \cos\theta_z \sin\theta_y & \cos\theta_z \sin\theta_x + \cos\theta_x \sin\theta_y \sin\theta_z & \cos\theta_x \cos\theta_y \end{pmatrix} \tag{11}$$

we use the first-order Taylor series approximation that is valid for small angles

$$\sin\theta \approx \theta - \frac{\theta^3}{3} + \frac{\theta^5}{5} - \cdots$$

$$\cos\theta \approx 1 - \frac{\theta^2}{2} + \frac{\theta^4}{4} - \cdots$$

and apply it to (11). The resulting approximative rotation is

$$\mathbf{R} \approx \begin{pmatrix} 1 & -\theta_z & \theta_y \\ \theta_x \theta_y + \theta_z & 1 - \theta_x \theta_y \theta_z & -\theta_x \\ \theta_x \theta_z - \theta_y & \theta_x + \theta_y \theta_z & 1 \end{pmatrix}. \tag{12}$$

As a second approximation we assume that the result of a multiplication of small angles yields even smaller values that can be omitted as well. This eliminates second-order and higher combination terms and Eq. (12) becomes:

$$\mathbf{R} \approx \begin{pmatrix} 1 & -\theta_z & \theta_y \\ \theta_z & 1 & -\theta_x \\ -\theta_y & \theta_x & 1 \end{pmatrix} = \mathbf{I}_{3\times3} + \begin{pmatrix} 0 & -\theta_z & \theta_y \\ \theta_z & 0 & -\theta_x \\ -\theta_y & \theta_x & 0 \end{pmatrix}. \tag{13}$$

We notice that this term is closely related to the Rodrigues formula but is no longer orthonormal.

Replacing this approximation (13) in the ICP error function Eq. (1) and rearranging the unknown variables in a vector yields:

$$\mathbf{m}_i - (\mathbf{R}\mathbf{d}_i + \mathbf{t}) \approx \mathbf{m}_i - \begin{pmatrix} 1 & -\theta_z & \theta_y \\ \theta_z & 1 & -\theta_x \\ -\theta_y & \theta_x & 1 \end{pmatrix} \mathbf{d}_i - \mathbf{t}$$

$$= \mathbf{m}_i - \mathbf{d}_i - \begin{pmatrix} 0 & d_{z,i} & -d_{y,i} & 1 & 0 & 0 \\ -d_{z,i} & 0 & d_{x,i} & 0 & 1 & 0 \\ d_{y,i} & -d_{x,i} & 0 & 0 & 0 & 1 \end{pmatrix} \begin{pmatrix} \theta_z \\ \theta_y \\ \theta_x \\ t_x \\ t_y \\ t_z \end{pmatrix}. \tag{14}$$

Surprisingly, the resulting equation is equal to the notation of Eq. (7) by Hofer and Pottmann [24,36]. The top part of the solution vector was called $\mathbf{c}$ while the bottom part resembles $\bar{\mathbf{c}}$. Therefore, the result has to be interpreted as a so-called helical motion and not using the small angle assumption. The small angle approximation fails, since the rotation calculated by the ICP algorithm always refers to the global coordinate system, i.e., represents a rotation about the origin $(0,0,0)$. While the helical motion takes care of this by calculating a rotation axis, our approximation does not regard this.

In order to make the small angle approximation of the rotation matrix Eq. (13) work, we have to apply the clever centroid trick, already used to derive Eq. (5). This separates the rotation from the translation. The resulting term is

$$\mathbf{m}_i' - \mathbf{R}\mathbf{d}_i' \approx \mathbf{m}_i' - \mathbf{d}_i' - \begin{pmatrix} 0 & d_{z,i}' & -d_{y,i}' \\ -d_{z,i}' & 0 & d_{x,i}' \\ d_{y,i}' & -d_{x,i}' & 0 \end{pmatrix} \begin{pmatrix} \theta_z \\ \theta_y \\ \theta_x \end{pmatrix}$$

Suppose the vector $\mathbf{u}$ to be $\mathbf{u} = (\theta_z, \theta_y, \theta_x)$. Then the optimal displacement for the ICP error function composed using the approximation in Eq. (14) is given by the solution to the following linear equation system:

$$\mathbf{D}_i = \begin{pmatrix} 0 & d'_{z,i} & -d'_{y,i} \\ -d'_{z,i} & 0 & d'_{x,i} \\ d'_{y,i} & -d'_{x,i} & 0 \end{pmatrix}$$

$$\sum_{i=1}^{N} \mathbf{D}_i^T \mathbf{D}_i \mathbf{u} = \sum_{i=1}^{N} \mathbf{D}_i^T (\mathbf{m}'_i - \mathbf{d}'_i)$$

After the approximation of the rotation is found, the optimal translation is calculated in Eq. (4).

3.2.3. Uncertainty-based registration

For some applications it is necessary to have a notion of the uncertainty of the poses calculated by the registration algorithm. The following is the extension of the probabilistic approach first proposed in [29] to 6 DoF. This extension is not straightforward, since the matrix decomposition, i.e., Eq. (16) cannot be derived from first principles. For a more detailed description of the extension refer to [8,9]. In addition to the pose $\mathbf{X}$, the pose estimate $\bar{\mathbf{X}}$ and the pose error $\Delta\mathbf{X}$ are required.

The positional error of a scan at its pose $\mathbf{X}$ is described by:

$$E = \sum_{i=1}^{m} \|\mathbf{X} \oplus \mathbf{d}_i - \mathbf{m}_i\|^2 = \sum_{i=1}^{m} \|\mathbf{Z}_i(\mathbf{X})\|^2$$

Here, $\oplus$ is the compounding operation that transforms a point $\mathbf{d}_i$ into the global coordinate system. For small pose errors $\Delta\mathbf{X}$, E can be linearized by use of a Taylor expansion:

$$\mathbf{Z}_i(\mathbf{X}) \approx \bar{\mathbf{X}} \oplus \mathbf{d}_i - \mathbf{m}_i - \nabla\mathbf{Z}_i(\bar{\mathbf{X}})\Delta\mathbf{X} = \mathbf{Z}_i(\bar{\mathbf{X}}) - \nabla\mathbf{Z}_i(\bar{\mathbf{X}})\Delta\mathbf{X}$$

Utilizing the matrix decomposition $\mathbf{M}_i\mathbf{H}$ of $\nabla\mathbf{Z}_i(\bar{\mathbf{X}})$ that separates the pose $\mathbf{X}$, which is contained in $\mathbf{H}$ from the points $\mathbf{m}_i$ and $\mathbf{d}_i$, which are contained in $\mathbf{M}_i$:

$$\mathbf{Z}_i(\mathbf{X}) \approx \mathbf{Z}_i(\bar{\mathbf{X}}) - \mathbf{M}_i\mathbf{H}\Delta\mathbf{X}$$

Appropriate decompositions are given for the Euler angles, quaternion representation and the Helix transform in the following paragraphs. Because $\mathbf{M}_i$ is independent of the pose, the positional error E is approximated as:

$$E \approx (\mathbf{Z} - \mathbf{M}\mathbf{H}\Delta\mathbf{X})^T (\mathbf{Z} - \mathbf{M}\mathbf{H}\Delta\mathbf{X}),$$

where $\mathbf{Z}$ is the concatenation of all $\mathbf{Z}_i(\bar{\mathbf{X}})$ and $\mathbf{M}$ the concatenation of all $\mathbf{M}_i$'s.

E is minimized by the ideal pose:

$$\bar{\mathbf{E}} = (\mathbf{M}^T\mathbf{M})^{-1}\mathbf{M}^T\mathbf{Z}$$

and its covariance is given by

$$\mathbf{C} = s^2(\mathbf{M}^T\mathbf{M}),$$

where s^2 is the unbiased estimate of the covariance of the identically, independently distributed errors of $\mathbf{Z}_i$:

$$s^2 = (\mathbf{Z} - \mathbf{M}\bar{\mathbf{E}})^T (\mathbf{Z} - \mathbf{M}\bar{\mathbf{E}})/(2m - 3). \qquad (15)$$

Note that $\bar{\mathbf{E}}$ is the minimum for the linearized pose $\mathbf{H}\Delta\mathbf{X}$. To obtain the optimal $\mathbf{X}$ the following transformation is performed:

$$\mathbf{X} = \bar{\mathbf{X}} - \mathbf{H}^{-1}\bar{\mathbf{E}},$$
$$\mathbf{C} = (\mathbf{H}^{-1})\mathbf{C}(\mathbf{H}^{-1})^T.$$

3.2.3.1. Euler angles.
The representation of pose $\mathbf{X}$ in Euler angles, as well as its estimate and error is as follows:

$$\mathbf{X} = \begin{pmatrix} t_x \\ t_y \\ t_z \\ \theta_x \\ \theta_y \\ \theta_z \end{pmatrix}, \bar{\mathbf{X}} = \begin{pmatrix} \bar{t}_x \\ \bar{t}_y \\ \bar{t}_z \\ \bar{\theta}_x \\ \bar{\theta}_y \\ \bar{\theta}_z \end{pmatrix}, \Delta\mathbf{X} = \begin{pmatrix} \Delta t_x \\ \Delta t_y \\ \Delta t_z \\ \Delta\theta_x \\ \Delta\theta_y \\ \Delta\theta_z \end{pmatrix}$$

The matrix decomposition $\mathbf{M}_i\mathbf{H} = \nabla\mathbf{Z}_i(\bar{\mathbf{X}})$, i.e., the Jacobian, is given by:

$$\mathbf{H} = \begin{pmatrix} 1 & 0 & 0 & 0 & \bar{t}_z\cos(\bar{\theta}_x)+\bar{t}_y\sin(\bar{\theta}_x) & \bar{t}_y\cos(\bar{\theta}_x)\cos(\bar{\theta}_y)-\bar{t}_z\cos(\bar{\theta}_y)\sin(\bar{\theta}_x) \\ 0 & 1 & 0 & -\bar{t}_z & -\bar{t}_x\sin(\bar{\theta}_x) & -\bar{t}_x\cos(\bar{\theta}_x)\cos(\bar{\theta}_y)-\bar{t}_z\sin(\bar{\theta}_y) \\ 0 & 0 & 1 & \bar{t}_y & -\bar{t}_x\cos(\bar{\theta}_x) & \bar{t}_x\cos(\bar{\theta}_y)\sin(\bar{\theta}_x)+\bar{t}_y\sin(\bar{\theta}_y) \\ 0 & 0 & 0 & 1 & 0 & \sin(\bar{\theta}_y) \\ 0 & 0 & 0 & 0 & \sin(\bar{\theta}_x) & \cos(\bar{\theta}_x)\cos(\bar{\theta}_y) \\ 0 & 0 & 0 & 0 & \cos(\bar{\theta}_x) & -\cos(\bar{\theta}_y)\sin(\bar{\theta}_x) \end{pmatrix} \qquad (16)$$

and

$$\mathbf{M}_i = \begin{pmatrix} 1 & 0 & 0 & 0 & -d_{y,i} & -d_{z,i} \\ 0 & 1 & 0 & d_{z,i} & d_{x,i} & 0 \\ 0 & 0 & 1 & -d_{y,i} & 0 & d_{x,i} \end{pmatrix}.$$

As required, $\mathbf{M}_i$ contains all point information while $\mathbf{H}$ expresses the pose information. Thus, this matrix decomposition constitutes a pose linearization similar to those proposed in the preceding sections. Note that, while the matrix decomposition is arbitrary with respect to the column and row ordering of $\mathbf{H}$, this particular description was chosen due to its similarity to the 3D pose solution given in [29].

3.2.3.2. Quaternions.
The representation of the pose $\mathbf{X}$ as quaternions, as well as its estimate and error are given as follows:

$$\mathbf{X} = \begin{pmatrix} t_x \\ t_y \\ t_z \\ p \\ q \\ r \\ s \end{pmatrix}, \bar{\mathbf{X}} = \begin{pmatrix} \bar{t}_x \\ \bar{t}_y \\ \bar{t}_z \\ \bar{p} \\ \bar{q} \\ \bar{r} \\ \bar{s} \end{pmatrix}, \Delta\mathbf{X} = \begin{pmatrix} \Delta t_x \\ \Delta t_y \\ \Delta t_z \\ \Delta p \\ \Delta q \\ \Delta r \\ \Delta s \end{pmatrix}$$

The matrix decomposition $\mathbf{M}_i\mathbf{H} = \nabla\mathbf{Z}_i(\bar{\mathbf{X}})$ for quaternions is given by:

$$\mathbf{M}_i = \begin{pmatrix} 1 & 0 & 0 & d_{x,i} & 0 & -d_{z,i} & d_{y,i} \\ 0 & 1 & 0 & d_{y,i} & d_{z,i} & 0 & -d_{x,i} \\ 0 & 0 & 1 & d_{z,i} & -d_{y,i} & d_{x,i} & 0 \end{pmatrix}$$

$$\mathbf{H} = \begin{pmatrix} \mathbf{I}_{3\times3} & -2\cdot\mathbf{T} \\ 0 & 2\cdot\mathbf{U} \end{pmatrix}$$

$$\mathbf{T}^T = \begin{pmatrix} \bar{p}\bar{t}_x+\bar{s}\bar{t}_y-\bar{r}\bar{t}_z & -\bar{s}\bar{t}_x+\bar{p}\bar{t}_y+\bar{q}\bar{t}_z & \bar{r}\bar{t}_x-\bar{q}\bar{t}_y+\bar{p}\bar{t}_z \\ \bar{q}\bar{t}_x+\bar{r}\bar{t}_y+\bar{s}\bar{t}_z & -\bar{r}\bar{t}_x+\bar{q}\bar{t}_y-\bar{p}\bar{t}_z & -\bar{s}\bar{t}_x+\bar{p}\bar{t}_y+\bar{q}\bar{t}_z \\ \bar{r}\bar{t}_x-\bar{q}\bar{t}_y+\bar{p}\bar{t}_z & \bar{q}\bar{t}_x+\bar{r}\bar{t}_y+\bar{s}\bar{t}_z & -\bar{p}\bar{t}_x-\bar{s}\bar{t}_y+\bar{r}\bar{t}_z \\ \bar{s}\bar{t}_x-\bar{p}\bar{t}_y-\bar{q}\bar{t}_z & \bar{p}\bar{t}_x+\bar{s}\bar{t}_y-\bar{r}\bar{t}_z & \bar{q}\bar{t}_x+\bar{r}\bar{t}_y-\bar{s}\bar{t}_z \end{pmatrix}$$

$$\mathbf{U} = \begin{pmatrix} \bar{p} & \bar{q} & \bar{r} & \bar{s} \\ \bar{q} & -\bar{p} & \bar{s} & -\bar{r} \\ \bar{r} & -\bar{s} & -\bar{p} & \bar{q} \\ \bar{s} & \bar{r} & -\bar{q} & -\bar{p} \end{pmatrix}$$

Again, all point information is restricted to $\mathbf{M}_i$ and all pose information to $\mathbf{H}$, so that the matrices describe a linearization of the quaternion transformation. Since this specific linearization was derived without regarding the normalized nature of the unit quaternions, this approach may yield non-unit quaternions. As non-unit quaternions do not constitute valid poses, the resulting quaternion must additionally be normalized before use.

4. n-Scan registration

The n-scan registration using linearization allows us to compute global optimal poses in one step given point correspondences between adjacent scans. These scans are given by a graph, where each link, $j \to k$ denotes a set of point pairs, i.e., closest points. Following the notation of ICP, scan j serves as the model set, while scan k serves as data set. Next we present four novel linear methods for the parameterization of the rotation.

4.1. Global registration using the helix transform

We minimize the error function for global consistent scan matching, i.e., we improve the approach given in [36] which is only locally consistent to include off-diagonal elements in the resulting system of equations [23]. The error function is extended to include all poses $\mathbf{X}_j = (\mathbf{x}_j^T, \, \bar{\mathbf{x}}_j^T)^T$:

$$E = \sum_{j \to k} \sum_i (\mathbf{m}_i - \mathbf{d}_i + (\bar{\mathbf{x}}_j + \mathbf{x}_j \times \mathbf{m}_i) - (\bar{\mathbf{x}}_k + \mathbf{x}_k \times \mathbf{m}_i))^2$$

$$= \sum_{j \to k} \left(\sum_i ((\bar{\mathbf{x}}_j + \mathbf{x}_j \times \mathbf{m}_i) - (\bar{\mathbf{x}}_k + \mathbf{x}_k \times \mathbf{m}_i))^2 + \sum_i 2((\mathbf{m}_i - \mathbf{d}_i) \right.$$

$$\left. \cdot \left(\bar{\mathbf{x}}_j + \mathbf{x}_j \times \mathbf{m}_i \right) + (\mathbf{d}_i - \mathbf{m}_i) \cdot (\bar{\mathbf{x}}_k + \mathbf{x}_k \times \mathbf{m}_i)) + \sum_i (\mathbf{m}_i - \mathbf{d}_i)^2 \right)$$

$$\text{(17)}$$

Reformulating E as

$$E = \mathbf{X}^T \cdot \mathbf{B} \cdot \mathbf{X} + 2\mathbf{A} \cdot \mathbf{X} + \sum_i (\mathbf{m}_i - \mathbf{d}_i)^2,$$

allows us to solve for the optimal poses $\mathbf{X}$ in the linear equation system:

$$\mathbf{B}\mathbf{X} = \mathbf{A}$$

$\mathbf{A}$ is attained as follows:

$$2\mathbf{A}\mathbf{X} = \sum_{j \to k} \sum_i 2((\mathbf{m}_i - \mathbf{d}_i)(\bar{\mathbf{x}}_j + \mathbf{x}_j \times \mathbf{m}_i) + (\mathbf{d}_i - \mathbf{m}_i)(\bar{\mathbf{x}}_k + \mathbf{x}_k \times \mathbf{m}_i))$$

$$\mathbf{A}_j = \sum_{j \to k} \sum_i \begin{pmatrix} \mathbf{m}_i \times (\mathbf{m}_i - \mathbf{d}_i) \\ \mathbf{m}_i - \mathbf{d}_i \end{pmatrix} + \sum_{k \to j} \sum_i \begin{pmatrix} \mathbf{m}_i \times (\mathbf{d}_i - \mathbf{m}_i) \\ \mathbf{d}_i - \mathbf{m}_i \end{pmatrix}$$

In other words, for each link $j \to k$ $\begin{pmatrix} \mathbf{m}_i \times (\mathbf{m}_i - \mathbf{d}_i) \\ \mathbf{m}_i - \mathbf{d}_i \end{pmatrix}$ is added to $\mathbf{A}_j$ while the same amount is subtract from $\mathbf{A}_k$.

$\mathbf{B}$ is defined by

$$\mathbf{X}^T \cdot \mathbf{B} \cdot \mathbf{X} = \sum_{j \to k} \sum_i ((\bar{\mathbf{x}}_j + \mathbf{x}_j \times \mathbf{m}_i) - (\bar{\mathbf{x}}_k + \mathbf{x}_k \times \mathbf{m}_i))^2,$$

and given as

$$\mathbf{B}_{j,j} = \sum_{\substack{j \to k \\ k \to j}} \sum_i \mathbf{M}_i$$

$$\mathbf{B}_{j,k} = \sum_{j \to k} \sum_i -\mathbf{M}_i,$$

where

$$\mathbf{M}_i = \begin{pmatrix} m_{y,i}^2 + m_{z,i}^2 & -m_{x,i}m_{y,i} & -m_{x,i}m_{z,i} & 0 & -m_{z,i} & m_{y,i} \\ -m_{x,i}m_{y,i} & m_{x,i}^2 + m_{z,i}^2 & -m_{y,i}m_{z,i} & m_{z,i} & 0 & -m_{x,i} \\ -m_{x,i}m_{z,i} & -m_{y,i}m_{z,i} & m_{x,i}^2 + m_{y,i}^2 & -m_{y,i} & m_{x,i} & 0 \\ 0 & m_{z,i} & -m_{y,i} & 1 & 0 & 0 \\ -m_{z,i} & 0 & m_{x,i} & 0 & 1 & 0 \\ m_{y,i} & -m_{x,i} & 0 & 0 & 0 & 1 \end{pmatrix}.$$

4.2. Global registration using the small angle approximation

Similarly to Eq. (17), the error metric is extended to include all poses $\mathbf{X}_j$:

$$E = \sum_{j \to k} \sum_i |\mathbf{R}_j \mathbf{m}_i + \mathbf{t}_j - (\mathbf{R}_k \mathbf{d}_i + \mathbf{t}_k)|^2.$$

Using the centroids $\mathbf{c}_d$ and $\mathbf{c}_m$, where $\mathbf{m}_i' = \mathbf{m}_i - \mathbf{c}_m$, $\mathbf{d}_i' = \mathbf{d}_i - \mathbf{c}_d$, E is restated as:

$$E = \sum_{j \to k} \sum_i |\mathbf{R}_j \mathbf{m}_i' + \mathbf{R}_j \mathbf{c}_m + \mathbf{t}_j - (\mathbf{R}_k \mathbf{d}_i' + \mathbf{R}_k \mathbf{c}_d + \mathbf{t}_k)|^2$$

$$= \sum_{j \to k} \sum_i |\mathbf{R}_j \mathbf{m}_i' - \mathbf{R}_k \mathbf{d}_i' - (\mathbf{t}_k - \mathbf{t}_j + \mathbf{R}_k \mathbf{c}_d - \mathbf{R}_j \mathbf{c}_m)|^2$$

$$= \sum_{j \to k} \left(\sum_i |\mathbf{R}_j \mathbf{m}_i' - \mathbf{R}_k \mathbf{d}_i'|^2 - 2 \sum_i (\mathbf{t}_k - \mathbf{t}_j + \mathbf{R}_k \mathbf{c}_d - \mathbf{R}_j \mathbf{c}_m) \right.$$

$$\left. \times (\mathbf{R}_j \mathbf{m}_i' - \mathbf{R}_k \mathbf{d}_i') + \sum_i |\mathbf{t}_k - \mathbf{t}_j + \mathbf{R}_k \mathbf{c}_d - \mathbf{R}_j \mathbf{c}_m|^2 \right).$$

The term $-2\sum_i (\mathbf{t}_k - \mathbf{t}_j + \mathbf{R}_k \mathbf{c}_d - \mathbf{R}_j \mathbf{c}_m)(\mathbf{R}_j \mathbf{m}_i' - \mathbf{R}_k \mathbf{d}_i')$ equates to zero, because all values refer to the centroids. This enables us to solve for the rotation of all poses independent of their translation.

4.2.1. Computing the rotation

Minimizing the first term of the restated error metric allows us to derive the optimal rotation of all poses. Since the rotation is a non-linear operation we utilize the following linearization: we apply the same small angle approximation as in Eq. (14):

$$\mathbf{R}_j \mathbf{m}_i = \begin{pmatrix} 0 & m_{z,i} & -m_{y,i} \\ -m_{z,i} & 0 & m_{x,i} \\ m_{y,i} & -m_{x,i} & 0 \end{pmatrix} \cdot \mathbf{X}_j + \mathbf{m}_i = \mathbf{M}_i \cdot \mathbf{X}_j + \mathbf{m}_i.$$

The rotation is represented as $\mathbf{X}_j = (\theta_{z,j}, \theta_{y,j}, \theta_{x,j})^T$. The following rotational error will be minimized:

$$E_R = \sum_{j \to k} \sum_i (\mathbf{M}_i \cdot \mathbf{X}_j - \mathbf{D}_i \cdot \mathbf{X}_k - (\mathbf{m}_i - \mathbf{d}_i))^2$$

$$= \sum_{j \to k} \sum_i (\mathbf{M}_i \cdot \mathbf{X}_j - \mathbf{D}_i \cdot \mathbf{X}_k)^2 + (\mathbf{m}_i - \mathbf{d}_i)^2$$

$$- 2(\mathbf{M}_i \cdot \mathbf{X}_j - \mathbf{D}_i \cdot \mathbf{X}_i) \cdot (\mathbf{m}_i - \mathbf{d}_i).$$

The error term is rewritten

$$E_R = \mathbf{X}\mathbf{B}\mathbf{X} + 2\mathbf{A}\mathbf{X} + (\mathbf{m}_k - \mathbf{d}_k)^2$$

in order to solve the linear equation system

$$\mathbf{B}\mathbf{X} + \mathbf{A} = 0.$$

With $\mathbf{B}$ given by:

$$\mathbf{B}_{j,j} = \sum_{j \to k} \sum_i \mathbf{D}_i^T \cdot \mathbf{D}_i + \sum_{k \to j} \sum_i \mathbf{M}_i^T \cdot \mathbf{M}_i$$

case $j < k$:

$$\mathbf{B}_{j,k} = -\sum_{j \to k} \sum_i \mathbf{M}_i^T \cdot \mathbf{D}_i$$

case $j > k$:

$$\mathbf{B}_{j,k} = -\sum_{j \to k} \sum_i \mathbf{D}_i^T \cdot \mathbf{M}_i,$$

and $\mathbf{A}$ by:

$$\mathbf{A}_j = \sum_{k \to j} \sum_i \begin{pmatrix} (m_{z,i} - d_{z,i}) \cdot d_{y,i} - (m_{y,i} - d_{y,i}) \cdot d_{z,i} \\ (m_{x,i} - d_{x,i}) \cdot d_{z,i} - (m_{z,i} - d_{z,i}) \cdot d_{x,i} \\ (m_{y,i} - d_{y,i}) \cdot d_{x,i} - (m_{x,i} - d_{x,i}) \cdot d_{y,i} \end{pmatrix}$$
$$- \sum_{j \to k} \sum_i \begin{pmatrix} (m_{z,i} - d_{z,i}) \cdot m_{y,i} - (m_{y,i} - d_{y,i}) \cdot m_{z,i} \\ (m_{x,i} - d_{x,i}) \cdot m_{z,i} - (m_{z,i} - d_{z,i}) \cdot m_{x,i} \\ (m_{y,i} - d_{y,i}) \cdot m_{x,i} - (m_{x,i} - d_{x,i}) \cdot m_{y,i} \end{pmatrix}$$

4.2.2. Computing the translation

With the optimal rotations successfully calculated, the optimal translation is determined by minimizing the term:

$$E_T = \sum_{j \to k} \sum_i (\mathbf{t}_k - \mathbf{t}_j + \mathbf{R}_k \mathbf{c}_d - \mathbf{R}_j \mathbf{c}_m)^2.$$

$\mathbf{R}_k \mathbf{c}_d - \mathbf{R}_j \mathbf{c}_m$ is abbreviated with $\mathbf{R}_{j,k}$:

$$E_T = \sum_{j \to k} \sum_i (\mathbf{t}_k - \mathbf{t}_j)^2 - 2(\mathbf{t}_k - \mathbf{t}_j)\mathbf{R}_{j,k} + \mathbf{R}_{j,k}^2.$$

Using the matrix notation:

$$E_T = \mathbf{T}^T \mathbf{B} \mathbf{T} + 2\mathbf{A}\mathbf{T} + \sum_{j \to k} \sum_i \mathbf{R}_{j,k}^2$$

this is achieved by solving the linear equation system:

$$\mathbf{B}\mathbf{T} + \mathbf{A} = 0$$

Here, $\mathbf{B}$ is given by:

$$\mathbf{B}_{j,j} = \sum_{\substack{j \to k \\ k \to j}} \mathbf{I}_{3 \times 3}$$

case $j < k$:

$$\mathbf{B}_{j,k} = -\sum_{j \to k} \mathbf{I}_{3 \times 3}$$

case $j > k$:

$$\mathbf{B}_{j,k} = -\sum_{j \to k} \mathbf{I}_{3 \times 3},$$

and $\mathbf{A}$ by:

$$\mathbf{A}_j = \sum_{j \to k} \mathbf{R}_j \mathbf{c}_m - \mathbf{R}_k \mathbf{c}_d - \sum_{k \to j} \mathbf{R}_j \mathbf{c}_m - \mathbf{R}_k \mathbf{c}_d.$$

4.3. Uncertainty-based global registration

Under the assumption that two poses $\mathbf{X}'_j$ and $\mathbf{X}'_k$ are related by the linear error metric $\mathbf{E}'_{j,k}$ we wish to minimize the Mahalanobis distance that describes the global error of all the poses:

$$W = \sum_{j \to k} (\overline{\mathbf{E}}_{j,k} - \mathbf{E}'_{j,k})^T \mathbf{C}_{j,k}^{-1} (\overline{\mathbf{E}}_{j,k} - \mathbf{E}'_{j,k})$$
$$= \sum_{j \to k} (\overline{\mathbf{E}}_{j,k} - (\mathbf{X}'_j - \mathbf{X}'_k)) \mathbf{C}_{j,k}^{-1} (\overline{\mathbf{E}}_{j,k} - (\mathbf{X}'_j - \mathbf{X}'_k)). \tag{18}$$

The error between two poses is modeled by the Gaussian distribution $(\overline{\mathbf{E}}_{j,k}, \mathbf{C}_{j,k})$. In matrix notation, W becomes:

$$W = (\overline{\mathbf{E}} - \mathbf{H}\mathbf{X})^T \mathbf{C}^{-1} (\overline{\mathbf{E}} - \mathbf{H}\mathbf{X}).$$

Here $\mathbf{H}$ is the signed incidence matrix of the pose graph, $\overline{\mathbf{E}}$ is the concatenated vector consisting of all $\overline{\mathbf{E}}'_{j,k}$ and $\mathbf{C}$ is a block-diagonal matrix comprised of $\mathbf{C}_{j,k}^{-1}$ as submatrices. Minimizing this function yields new optimal pose estimates. The minimization of $\mathbf{W}$ is accomplished via the following linear equation system:

$$(\mathbf{H}^T \mathbf{C}^{-1} \mathbf{H})\mathbf{X} = \mathbf{H}^T \mathbf{C}^{-1} \overline{\mathbf{E}}$$
$$\mathbf{B}\mathbf{X} = \mathbf{A}.$$

The matrix $\mathbf{B}$ consists of the submatrices

$$\mathbf{B}_{j,k} = \begin{cases} \sum_{k=0}^n \mathbf{C}_{j,k}^{-1} & (j = k) \\ \mathbf{C}_{j,k}^{-1} & (j \neq k). \end{cases}$$

The entries of $\mathbf{A}$ are given by:

$$A_j = \sum_{\substack{k=0 \\ k \neq j}}^n \mathbf{C}_{j,k}^{-1} \overline{\mathbf{E}}_{j,k}.$$

In addition to $\mathbf{X}$, the associated covariance of $\mathbf{C}_X$ is computed as follows:

$$\mathbf{C}_X = \mathbf{B}^{-1}$$

The actual positional error of two poses $\mathbf{X}_j$ and $\mathbf{X}_k$ is not linear:

$$E_{j,k} = \sum_{i=1}^m \|\mathbf{X}_j \oplus \mathbf{d}_i - \mathbf{X}_k \oplus \mathbf{m}_i\|^2 = \sum_{i=1}^m \|\mathbf{Z}_i(\mathbf{X}_j, \mathbf{X}_k)\|^2.$$

Analogous to the simple 2-scan case the linearized pose difference $\mathbf{E}'_{j,k}$ is obtained by use of a Taylor expansion of $\mathbf{Z}_i(\mathbf{X}_j, \mathbf{X}_k)$:

$$\mathbf{Z}_i(\mathbf{X}_j, \mathbf{X}_k) \approx \mathbf{Z}_i(\overline{\mathbf{X}}_j, \overline{\mathbf{X}}_k) - \left(\nabla_{\mathbf{X}_j} \mathbf{Z}_i(\overline{\mathbf{X}}_j, \overline{\mathbf{X}}_k) \Delta \mathbf{X}_j - \nabla_{\mathbf{X}_k} \mathbf{Z}_i(\overline{\mathbf{X}}_j, \overline{\mathbf{X}}_k) \Delta \mathbf{X}_k \right).$$

Here, $\nabla_{\mathbf{X}_j}$ refers to the derivative with respect to $\mathbf{X}_j$. Utilizing the same matrix decomposition $\mathbf{M}_i \mathbf{H}$ of $\nabla \mathbf{Z}_i(\overline{\mathbf{X}})$ as in the 2-scan case $\mathbf{Z}_i(\mathbf{X}_j, \mathbf{X}_k)$ is approximated as:

$$\mathbf{Z}_i(\mathbf{X}_j, \mathbf{X}_k) \approx \mathbf{Z}_i(\overline{\mathbf{X}}_j, \overline{\mathbf{X}}_k) - \mathbf{M}_i \mathbf{E}'_{j,k},$$

where $\mathbf{E}'_{j,k}$ is the linear error metric given by:

$$\mathbf{E}'_{j,k} = (\mathbf{H}_j \Delta \mathbf{X}_j - \mathbf{H}_k \Delta \mathbf{X}_k) = (\mathbf{X}'_j - \mathbf{X}'_k).$$

$\mathbf{E}'_{j,k}$ is linear in the quantities $\mathbf{X}'_j$ that will be estimated by the algorithm. Again, the minimum of $\mathbf{E}'_{j,k}$ and the corresponding covariance are given by

$$\overline{\mathbf{E}}_{j,k} = (\mathbf{M}^T \mathbf{M})^{-1} \mathbf{M}^T \mathbf{Z}$$

$$\mathbf{C}_{j,k} = s^2 (\mathbf{M}^T \mathbf{M}).$$

Here $\mathbf{Z}$ is the concatenated vector consisting of all $\mathbf{Z}_i = \overline{\mathbf{X}}_j \oplus \mathbf{d}_i - \overline{\mathbf{X}}_k \oplus \mathbf{m}_i$.

Note that the results have to be transformed in order to obtain the optimal pose estimates, just like in the simple 2-scan case.

$$\mathbf{X}_j = \overline{\mathbf{X}}_j - \mathbf{H}_j^{-1} \mathbf{X}'_j,$$

$$\mathbf{C}_j = (\mathbf{H}_j^{-1}) \mathbf{C}_j^X (\mathbf{H}_j^{-1})^T.$$

Table 1
Overview of the complexity of *n*-scan registration methods. *n* denotes the number of 3D scans.

Registration algorithm	Number of equations
Helix transform	$(6n)^3$
Small angle approximation	$(3n)^3 + (3n)^3$
Uncertainty-based (Euler)	$(6n)^3$
Uncertainty-based (quaternion)	$(7n)^3$

5. Summary of *n*-scan registration methods

In the previous section we have derived different global registration methods. We assumed to have a network of overlapping scans. All methods have in common that the problem is reduced to solving a system of linear equations. Table 1 summarizes the computational complexity of the presented methods. It presents the number of linear equations to be solved. *Note:* With growing
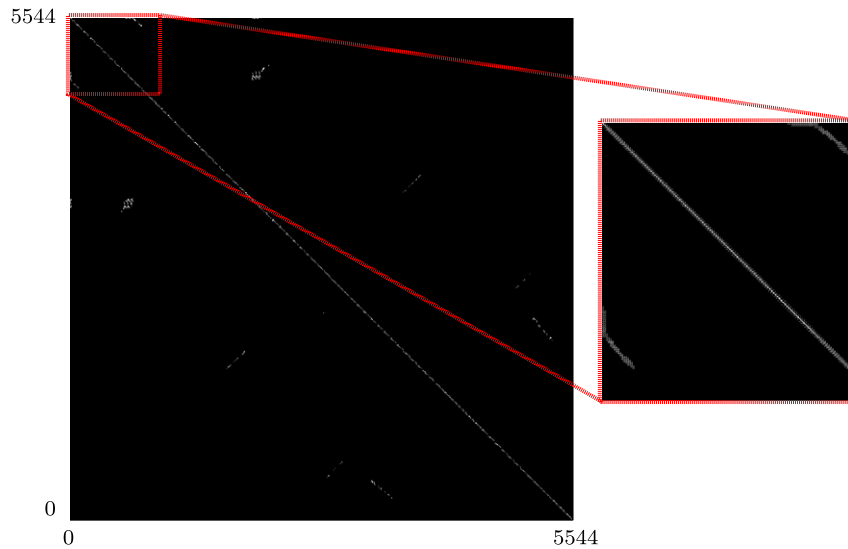

Fig. 5. Sparse matrix of the linear system of equations. Matrix entries that are not zero are printed in white. This matrix occurs when optimizing over all 3D scans of the scene presented in Fig. 1.
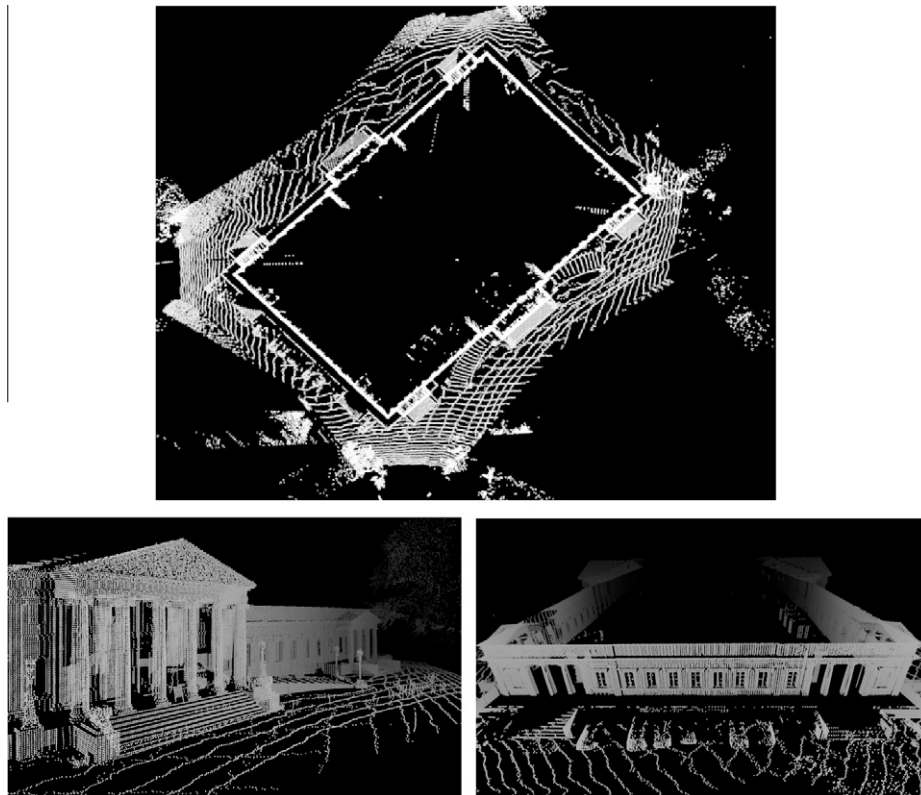

Fig. 6. The data set Rosenstein palace. Top: Bird eye view. Bottom: 3D views.

Fig. 7. Top left: Schema of the airborne based acquisition of reference data. Top right: 3D map consisting of aerial laser data and extrapolated 2D reference data. Bottom: Airborne and 3D map (black) with superimposed 3D scans (gray).
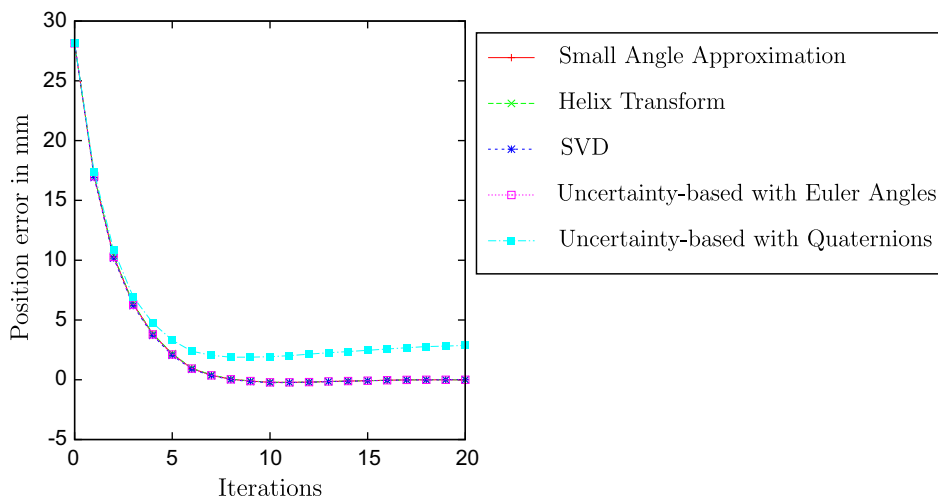

Fig. 8. Convergence of the registration of two scans using different algorithms.

3D scene sizes the constants usually hidden in the Landau notation are important in practical applications.

The appendix contains the proofs that the resulting linear system can be solved by a Cholesky decomposition, since it is positive definite. Furthermore, in practical applications it turns out that the matrix is sparse (cf. Fig. 5). Therefore, algorithms for solving sparse systems, i.e., the sparse Cholesky decompositions are applicable [13].

6. Experiments and results

6.1. Registration of terrestrial 3D laser scans

Initial tests have been carried out with data obtained from Rosenstein palace, near Stuttgart using a Leica HDS 3000 laser scanner [40]. The data set consists of five 3D scans covering all sides of the palace. After a visual inspection of the scan matching

Table 2
Run time comparison (Intel(R) Q9450 at 2.66 GHz, single threaded) for our linear solutions for the 2-Scan problem in comparison to closed form solutions. The timing for Rosenstein palace have been averaged over 4 3D-scan registrations. The data of the set HANNOVER2 were reduced using an octree with edge-length 10 cm and averaged over 923 scan registrations. Significant run time improvements are obtained in the *n* scan case (see also Tables 1 and 3).

Registration algorithm	Run time (Rosenstein palace)	Run time (HANNOVER2)
Helix Transform	2.232 s	0.1407 s
Small Angle Approximation	2.230 s	0.1402 s
Uncertainty-Based (Euler)	2.437 s	0.1581 s
Uncertainty-Based (quaternion)	2.388 s	0.1450 s
Closed form (SVD) [1]	2.502 s	0.1803 s
Closed form (quaternion) [25]	2.475 s	0.1613 s

result, e.g., as given in Fig. 6 we made the conclusion that all the linearization methods are in principle able to correctly match 3D scans globally.

Next, we aim to systematically evaluate 3D scan matching as it appears in practical applications. Unfortunately, a simulated evaluation of the minimization step, i.e., using a randomly generated point cloud as a source for several 3D scans with small errors in their poses is infeasible. The usual procedure is to minimize the error metric in the proposed fashion using perfect point correspondences, thus eliminating any error introduced by incorrect point pairs. Since locally accumulating minimization errors lead to incorrect correspondences, this unfairly rewards local approaches while global registration algorithms are penalized.
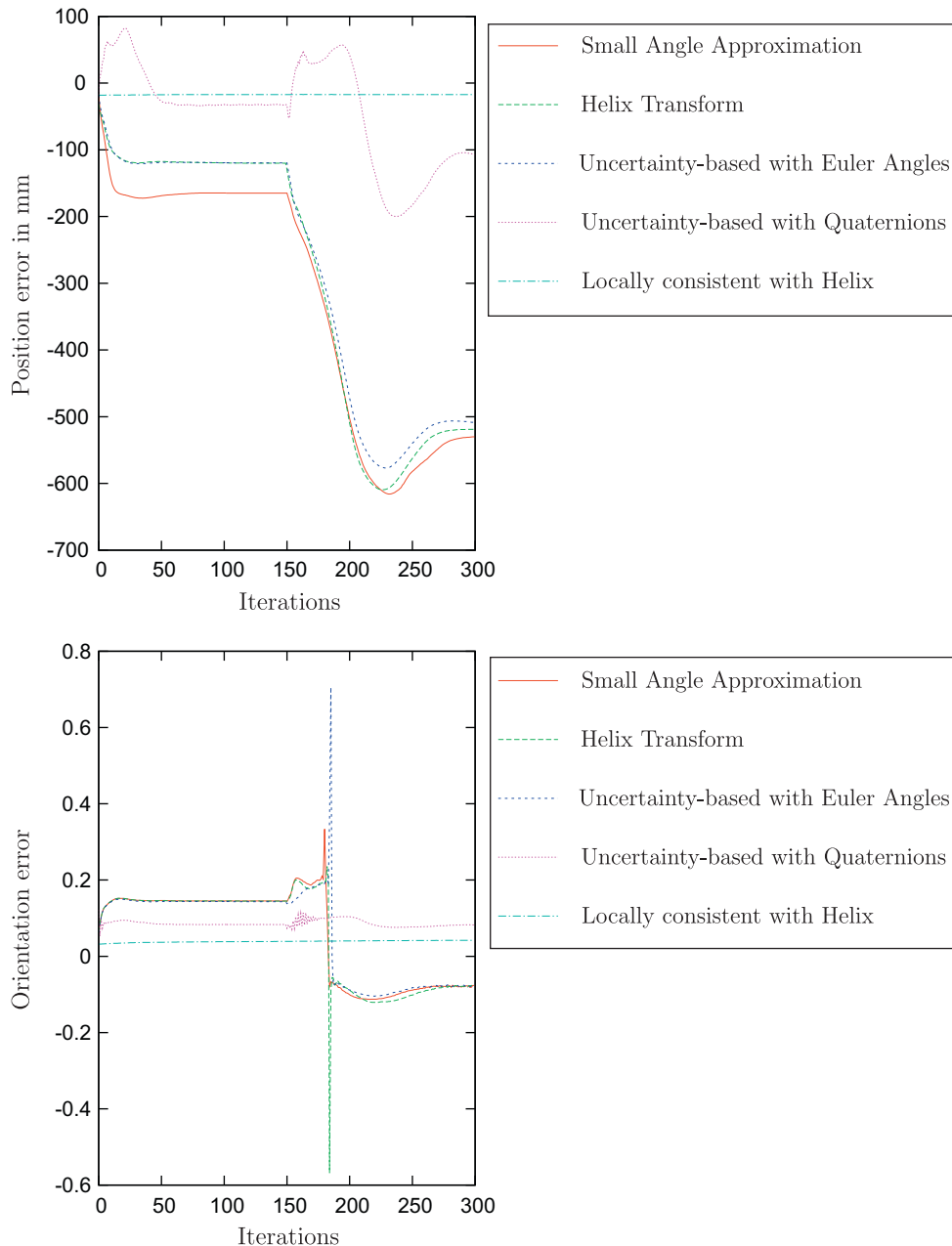

Fig. 9. Convergence of the registration of scan number 80 (top: translational error, bottom: rotational error) using different minimization algorithms. The first 150 iterations correspond to the first relaxation (trajectory A-B-C-D-A-B) while the second 150 iterations represent the result after registration of 384 3D scans (trajectory A-B-C-D-A-B-E-F-A).
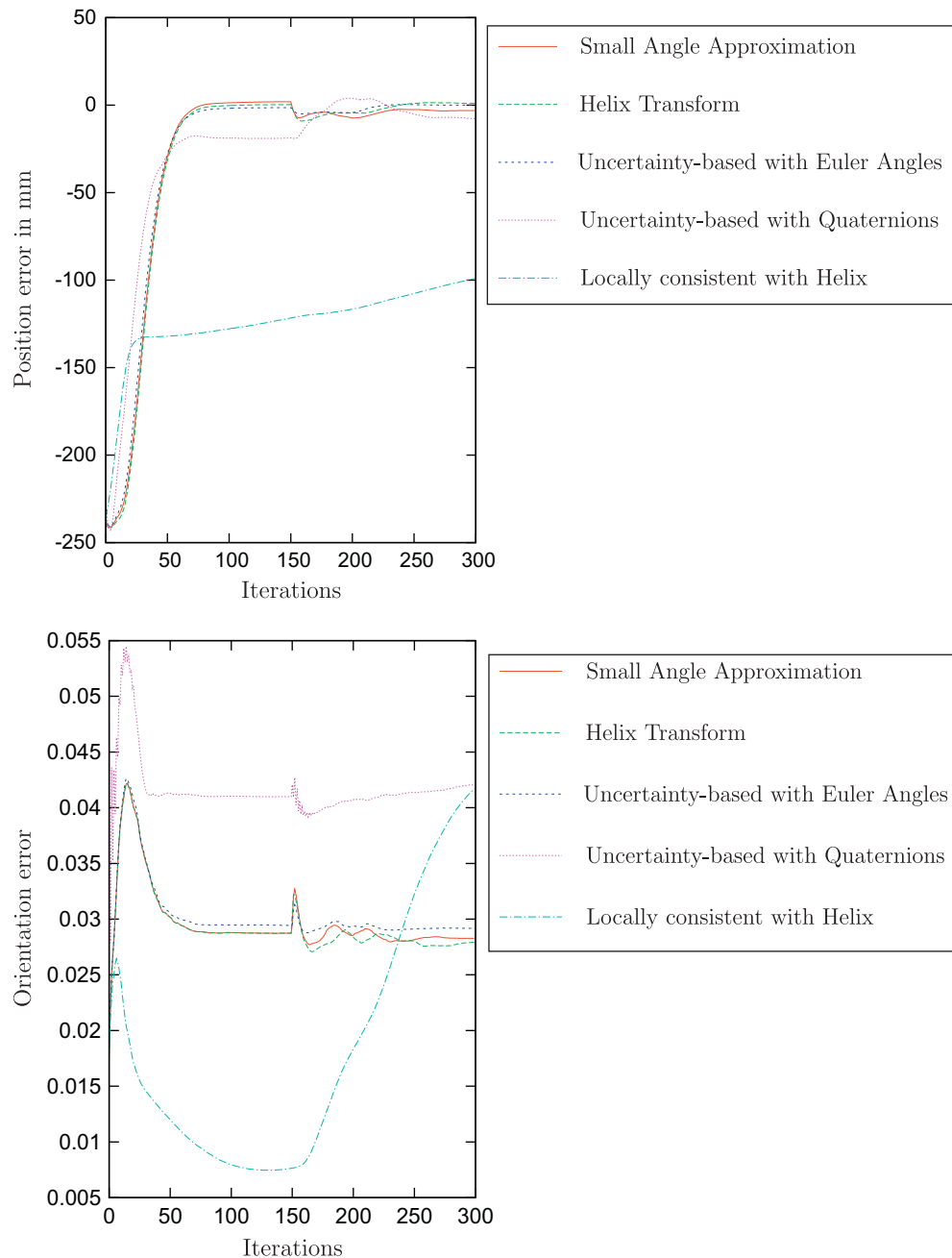
Fig. 10. Same as Fig. 9 but for scan number 150 using the different minimization algorithms.

6.2. Systematic tests in an urban environment

These experiments have been made using the data of the Robotic 3D Scan Repository [52]. Implementations of the four methods can be found in [55]. The data set HANNOVER2 (cf. Fig. 2) has been acquired in an urban area and contains 924 3D scans each containing up to 35,000 3D data points. It was acquired by a robot carrying a continuously rotating 3D scanner [49]. For the data set HANNOVER2 ground truth data in form of a 2D map provided by the German land registry office (KataSTERamt) is available. This map contains the buildings with a precision of 1 cm. This quality was ensured at the time the map was generated by geodesy using conventional surveying equipment. In addition, we obtained airborne based 3D data. The accuracy of the airborne data is in the cm range, too, since a precise DGPS and IMU in combination with a 2D airborne scanner has been used. Based on this data so-called reference data is gen-

erated as follows (see Fig. 7): the 2D map contains lines representing buildings and it is extrapolated to 3D by creating 3D points, i.e., for every line, we generate 3D points from the ground level up to 10 m with a 25 cm discretization. These 3D points are fused with the 3D data from the airplane. The result is a precise 3D reference map. Using this 3D reference map, we generate ground truth poses for all 924 3D laser scans by matching the scans with the reference map. To these poses we will refer to as "ground truth".

6.2.1. Registration of two scans

We analyzed the registration of two 3D scans to ensure our methods work correctly. Fig. 8 shows the convergence of the ICP algorithm using the different minimization algorithms. The helix transform, the small angle approximation, and the uncertainty-based optimization using Euler angles behave like the closed-form solutions, i.e., the value of the error function Eq. (1) is identical to
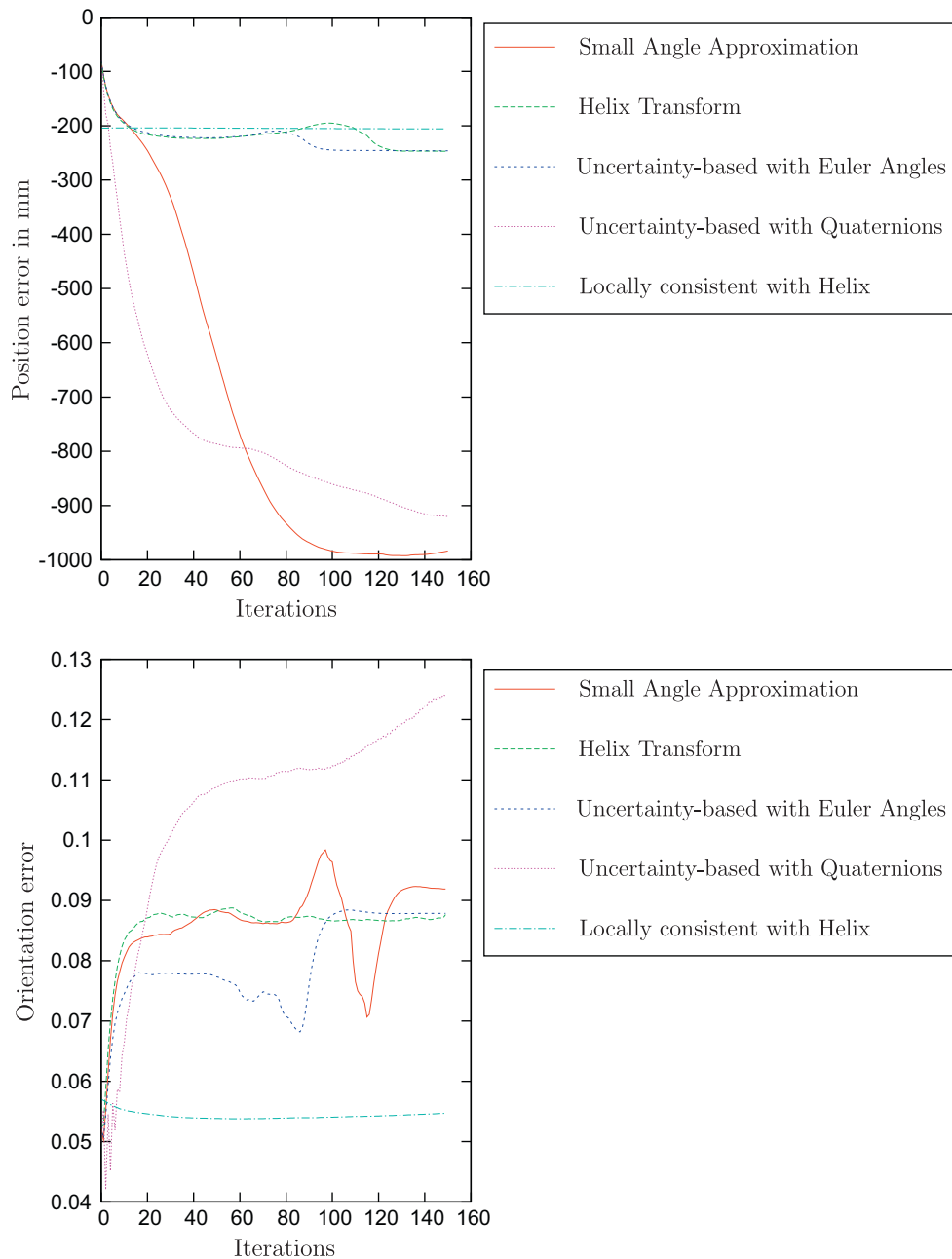
Fig. 11. Convergence of the registration of scan number 200 (top: translational error, bottom: rotational error) using different minimization algorithms. These 150 iterations correspond to the second relaxation (sequence: A-B-C-D-A-B-E-F-A).

the closed-form solution. Thus the convergence speed and the final pose are equal. The convergence graphs from the remaining 923 registrations are similar to the one presented in Fig. 8. We conclude, that the step length computed by our linearized methods are close to the optimal step length. For the experiments we used a maximal point-to-point distance threshold of 25 cm. However, the quaternion based method shows slightly different behavior, which is due to the fact that it requires normalization afterward.

Table 2 shows the computational requirements for our linear solutions in comparison with the SVD [1] and quaternion non-linear solution [25]. The runtime is averaged over ten runs over the whole data set (5 scans Rosenstein palace, 924 scans HANNOVER2). The closed-form solutions are slightly outperformed by the linear ones, since only a linear system of equations has to be solved using the Cholesky decomposition. Since Uncertainty-based (Euler)

computation requires the computation of sine and cosine it is slightly less performant.

6.2.2. Registration of n-scans

We compared the incrementally used ICP algorithm by matching a sequence of 924 3D scans (a video is given using the following link: http://plum.eecs.jacobs-university.de/submissions/large_slam.mpg). Here we matched every 3D scan against its predecessor and take into account that errors sum up. After we returned with the scanner to the origin a loop was closed. We applied the global relaxation and analyzed the error function minimization. Fig. 9 and Fig. 10 presents the results for two 3D scans (Nos. 80 and 150). The figures show the position error of these scans (top) that was computed using the difference to the reference position and the orientational error (bottom) that was computed by first calculating the rotation needed
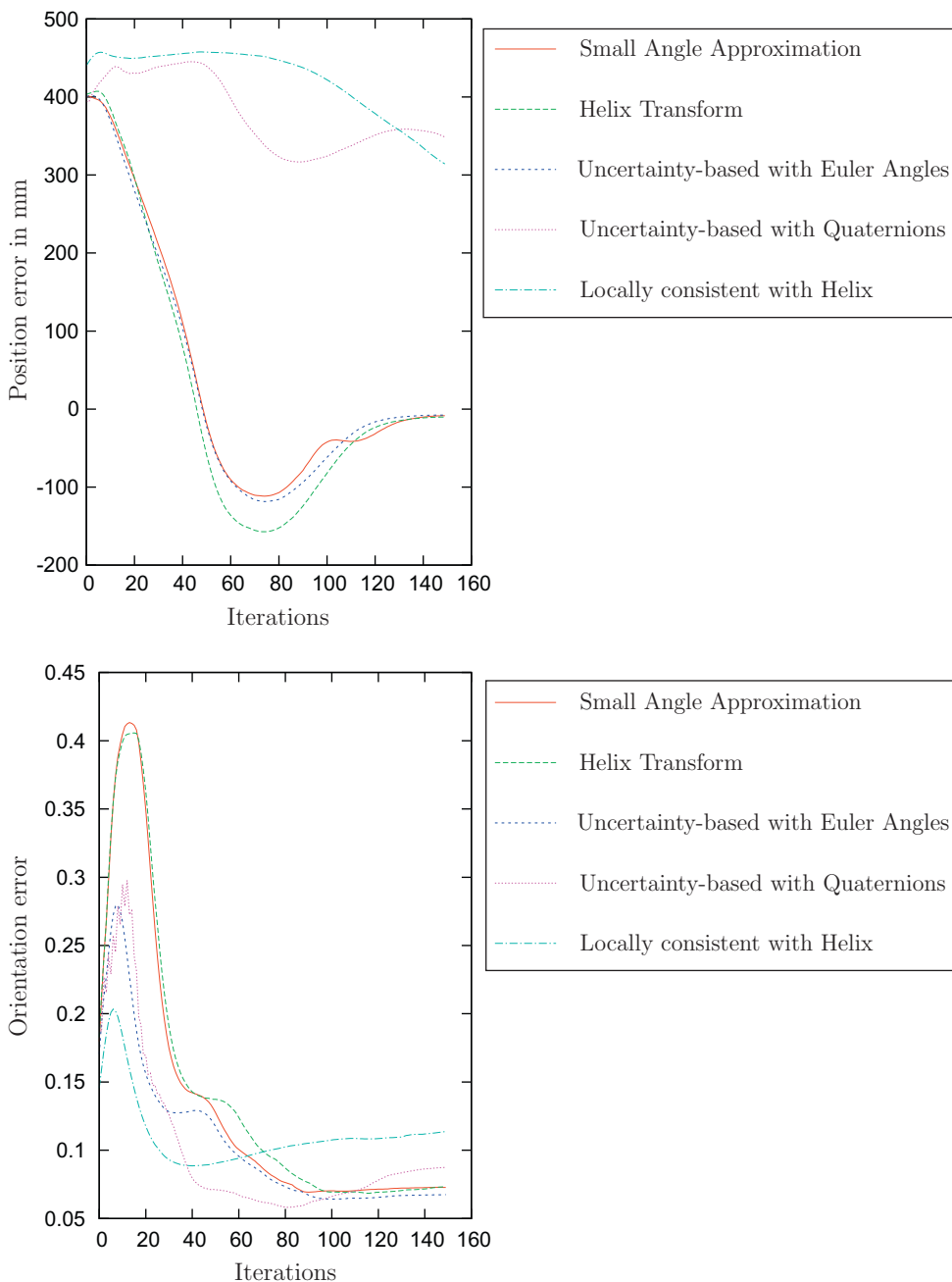
Fig. 12. Same as Fig. 11 but for scan number 384 using the different minimization algorithms.

to map the scan matching result to the reference orientation and then computing the axis-angle representation. The resulting angle describes the made error. The figures report the error for two loop closings, i.e., the first relaxation was up to iteration 150, the second one up to iteration 300. In Fig. 9 the optimization starts with a correct guess, and the scans are moved to gain a better mutual fit, but relocates them away from ground truth. The ground truth poses are *unknown* to the optimization process. In Fig. 10, we see that all methods converge to stable different minima and with the exception of the quaternion algorithm, the final minimum is close to the ground truth.

The first loop uses the first 150 3D scans. Scan No. 80 (cf. Fig. 9) resides in the middle of the loop. Following the analogy of the spring system (cf. Fig. 3) scans in the middle of the loops are moved only very slowly, since the main inconsistencies occur at the loop

closing, e.g., at Scan No. 150 (cf. Fig. 10) and this needs to be propagated through the whole spring system.

Figs. 11 and 12 show the precision of two 3D scans that reside in the second loop closing. Two methods, namely the small angle approximation and the uncertainty-based quaternion solution show convergence to incorrect minima for scan No. 200, while for scan No. 384 only the quaternion solutions seams to be incorrect. Note that the error of the small angle approximation is due to misalignment errors on the *y*-coordinate, i.e., the height of the scans.

The best performance in terms of position accuracy is achieved by the helix transform and the uncertainty-based optimization using Euler angles (cf. Fig. 13 and Table 3). As expected, globally consistent scan matching reduces the position error at the positions, where the loop is closed, e.g., Fig. 13 at scan index 100, where
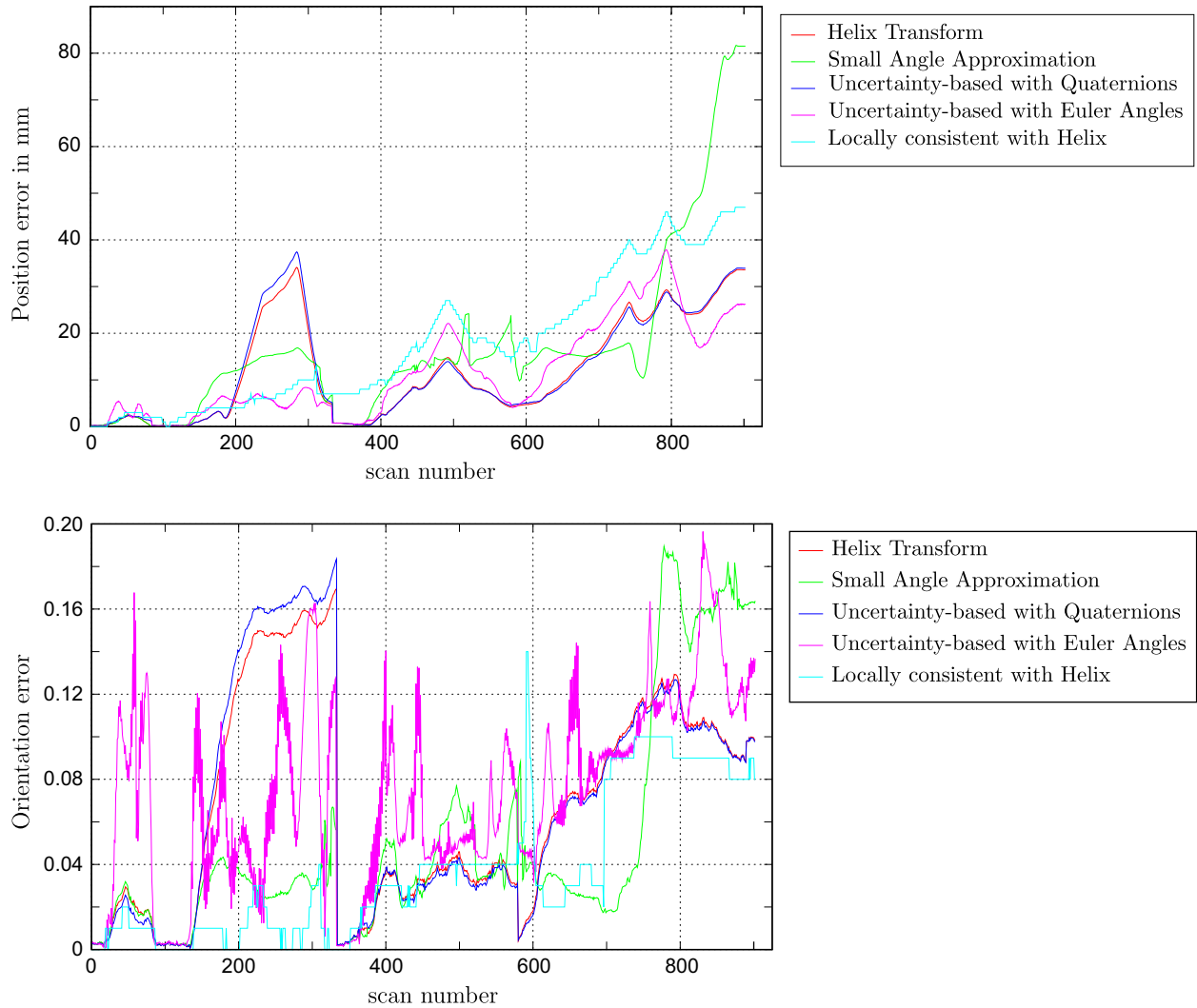
Fig. 13. Final error, after sequential registration of all 3D scans and globally consistent scan matching (distance to ground truth positions (top) and rotational error (bottom)) (see Fig. 1 and the corresponding video).

Table 3
Run times and final summed error over all 924 3D scans. Run times apply only for the SLAM back-end and were taken on an Intel(R) Q9450 at 2.66 GHz, using single threaded computations.

Registration algorithm	Run time	Summed position error	Summed orientation error
Helix transform	44.134 s	10418.54	6263.81
Small angle approximation	34.001 s	11026.47	6235.12
Uncertainty-based (Euler)	50.459 s	10819.15	6133.44
Uncertainty-based (quaternion)	84.592 s	15261.31	4635.24
Locally consistent with helix	40.103 s	16411.85	3813.83

the first loop was closed and at the indices 300–400 and 600–700. The locally consistent reference method shows increasing error.

The rotational error is low for all relaxation methods. The reason for this is that the used starting guesses for optimization are already quite good as they are produced by the locally applied ICP algorithm and the IMU starting guess. Please refer to [8] for more details for the system overview. The rotational errors have a large variation range and are therefore hard to judge.

Run times for the benchmarking data set are also given in Table 3. In terms of run time, the small angle approximation outperforms all

other methods due to the small number of equations in the linear system (see Table 1) and the simple computing scheme for the matrix entries. The uncertainty-based methods are not so performant due to the additionally required computations like the transformation of the poses with matrix **H**. Please note, the overall run time is dominated by the search for closest points, which is not given in the table.

We have made experiments with iterating the minimization of the global error function, without re-searching for closest points. This approach is used by bundle adjustment [46] to find a good minimum. Since no major pose changes are computed further iterations, we conclude, that the computed step length is close to the optimal one. The one-step solution using new closest points is more effective.

Additional experiments for the registration of n scans with other data sets provided by the Robotic 3D Scan Repository [52] support the statement, that the helix transform and the uncertainty based optimization using Euler angles perform best.

6.3. Interpretation of the results

The experiments show that global registration of many 3D scans yield a complex and fragile optimization system. Small variances in the calculated matrices yield different closest point

pairs in the following iteration, which in turn result in different matrices. Most stable results with respect to the final pose estimates of the 3D scans can be reported for the approximation of the error function using the helix transform and the uncertainty-based optimization using Euler angles. The quaternion based approach needs a re-normalization step to compute orthonormal rotation matrices, i.e., it leaves the group of rotations. Thus, it is most likely to fail and we do not recommend using it. Table 4 shows our judgment of the difficulty to deriving the linearization and implementing it.

All minimization algorithms deform the map while optimizing, such that the outer parts of the map, i.e., the height of the regions close to C, L and I are raised. After several optimization steps the map converges due to the iterative fashion of the algorithm. Linearization usually has the effect that mapped loops are too large [18]. The local optimal reference method do not make major changes to the locations of scans and the result using this method largely depends on the quality of initial pose guesses (see also Fig. 3, left).

Our experiments have shown that the helix transform performs qualitatively as good as the uncertainty-based algorithm using Euler angles. Thus, we now propose a novel algorithm that combines the positive aspects, i.e., we develop an uncertainty-based helix registration method.

7. An uncertainty-based registration using the helix transform

The detailed analysis above has motivated the idea of an uncertainty-based algorithm using the helical motion. As with the uncertainty-based registration with Euler angles or quaternions the Mahalanobis distance Eq. (18) is minimized in order to compute the global pose estimates and their covariances. The minimum is given as the solution to the linear equation system $\mathbf{BX} = \mathbf{A}$, where $\mathbf{B}$ and $\mathbf{A}$ are constructed with the quantities $\overline{\mathbf{E}}_{j,k}$ and $\mathbf{C}_{j,k}^{-1}$ as in Section 4.3. $\overline{\mathbf{E}}_{j,k} = (\mathbf{M}^T\mathbf{M})^{-1}\mathbf{M}^T\mathbf{Z}$ and $\mathbf{C}_{j,k}^{-1} = s^2(\mathbf{M}^T\mathbf{M})$ are calculated according to the corrected values for $\mathbf{M}$ and $\mathbf{Z}$ that follow from the derivation for the Helix transform error metric:

$$E = \sum_{j \to k} \sum_i \left\| \mathbf{m}_i - \mathbf{d}_i + (\bar{\mathbf{x}}_j + \mathbf{x}_j \times \mathbf{m}_i) - (\bar{\mathbf{x}}_k + \mathbf{x}_k \times \mathbf{m}_i) \right\|^2$$
$$= \sum_{i=1}^m \left\| \mathbf{Z}_i(\mathbf{X}_j, \mathbf{X}_k) \right\|^2.$$

Since the derivation is identical to the one in Section 4.3 we give the matrix decomposition that is central for calculating $\overline{\mathbf{E}}_{j,k}$ and $\mathbf{C}_{j,k}^{-1}$:

$$\mathbf{M}_i = \begin{pmatrix} 0 & m_{z,i} & -m_{y,i} & 1 & 0 & 0 \\ -m_{z,i} & 0 & m_{x,i} & 0 & 1 & 0 \\ m_{y,i} & -m_{x,i} & 0 & 0 & 0 & 1 \end{pmatrix}$$
$$\mathbf{H} = \mathbf{I}_{6 \times 6}.$$

Comparing both helix transform based registrations reveals that the only difference is that the uncertainty-based registration introduces the value s^2, see Eq. (15), which scales the covariances. For a constant s over all pairs or the simple 2-scan case the solution given by the non-uncertainty-based registration is identical to the one without using uncertainties.

8. Conclusions and outlook

This paper contained three major contributions: firstly, we summarized existing locally and globally optimal scan matching methods and extended them by a working global helix-based registration, by a small angle approximation, and an uncertainty-based registration using the helix transform. All methods approximate a closed-form solution for iterative closest point algorithms. As our experiments have demonstrated, it is not recommended to use the uncertainty-based registration using quaternions, since it does not stay in the $SO(3)$ group and requires re-normalization. Secondly, we discussed the run time of the algorithms by stating the number of equations that have to be solved. Thirdly, we exhaustively evaluated the global scan matching by comparing scan poses with a genuine truth and discussed the outcomes. A minor contribution of the paper is that we showed the linear system of equations is for the registration using the helix transform is equal to the system one derives when using the small angle approximation. Another minor contribution is that we have demonstrated that the use of the helix transform in a probabilistic context changes the system of equations only by a scaling factor.

The presented algorithms establish the foundation for mapping in 3D using 3D laser scanners. The applications are large scale systems ranging from terrestrial laser scanning, survey and geodesy to robotic mapping. In the latter research field probabilistic methods are state of the art [42]. This paper has showed, that deterministic modelings of the scan registration problem, i.e., by using the helix transform, yield the same performance as probabilistic ones, i.e., uncertainty-based optimization using Euler angles or differ only about a constant factor, for example the uncertainty-based optimization using the helix transform.

Needless to say a lot of work remains to be done. In future work we are aiming at finding a closed-form solution to get rid of the linearization and the problems due to it. Section 3.1 outlines the math for the two-scan case. The open question remains, if such methods are extendable to multiple scan registrations. Initial progress is available here by Yguel, who derived a closed-form solution for the 2-scan registration problem, incorporating the Mahalanobis distance [50].

Furthermore, in future work we plan to apply the proposed algorithms to large scale experiments, i.e., to 3D mapping of cities. Then, the back-end, i.e., solving the system of linear equations becomes the bottleneck, while it is currently the front-end search for closest points, i.e., $n \ll N$, where n is the number of poses and N is the number of 3D points per scan. This will need to include recent results from the SLAM community, e.g., the work presented in [17,34,35] that aim to reduce the run time of the SLAM back-end. In this paper we used CSPARSE, a sparse Cholesky decomposition, to speed up the matrix operations [13,9].

Table 4
Difficulty of deriving and implementing a global optimal solution. Straightforward calculations and implementations are marked with "+", while more difficult approaches are marked with "−".

Registration algorithm	Deriving the solution	Implementation simplicity
Helix transform	+	+
Small angle approximation	++	++
Uncertainty-based (Euler)	− −	+
Uncertainty-based (quaternion)	−	+

and Claus Brenner (Leibniz University of Hannover) for letting us use the airborne 3D data.

Appendix A

For all registration algorithms described in this paper, some matrix $\mathbf{B}$ is inverted. Because these matrices can become very large, it is desirable to use fast matrix inversion techniques such as the Cholesky decomposition. In order for this to be effective, the matrix in question needs to be positive definite. The following sections provide proofs of this property for each registration algorithm. In each section the notation for the respective algorithms are utilized.

A.1. Helix transform

$\mathbf{B}$ is by the definition:

$$\mathbf{X}^T \cdot \mathbf{B} \cdot \mathbf{X} = \sum_{j \to k} \sum_i ((\bar{\mathbf{c}}_j + \mathbf{c}_j \times \mathbf{m}_i) - (\bar{\mathbf{c}}_k + \mathbf{c}_k \times \mathbf{m}_i))^2 \geqslant 0$$

positive semi definite. Since any n-scan problem includes the link $0 \to 1$ it is sufficient to show

$$\sum_i (\bar{\mathbf{c}}_1 + \mathbf{c}_1 \times \mathbf{m}_i)^2 \neq 0,$$

for all $\mathbf{c}_1, \bar{\mathbf{c}}_1 \neq 0$. The solution space of $\bar{\mathbf{c}}_1 + \mathbf{c}_1 \times \mathbf{m}_i = 0$ is in the form of two lines parallel to $\mathbf{c}_1$. In practice no 3D scan satisfies such a condition.

A.2. Small angle approximation

The solution matrix $\mathbf{B}$ for the rotation is positive semi definite by definition:

$$\mathbf{X}^T \cdot \mathbf{B} \cdot \mathbf{X} = \sum_{j \to k} \sum_i (\mathbf{M}_i \cdot \mathbf{X}_j - \mathbf{D}_i \cdot \mathbf{X}_k)^2 (\mathbf{m}_i - \mathbf{d}_i).$$

It is only necessary to show

$$\sum_i (\mathbf{D}_i \cdot \mathbf{X}_1)^2 > 0$$

or equivalently

$$\sum_i \mathbf{X}_1 \times \mathbf{d}_i \neq 0,$$

for all $\mathbf{X}_1 \neq 0$. This holds true for all $\mathbf{d}_i \neq 0$.

The matrix $\mathbf{B}$ that is required for the recovery of the translation is defined by:

$$\mathbf{X}^T \cdot \mathbf{B} \cdot \mathbf{X} = \sum_{j \to k} \sum_i (\mathbf{t}_k - \mathbf{t}_j)^2.$$

This is always greater than zero for any $\mathbf{t}_k \neq \mathbf{t}_j$. Since $\mathbf{t}_0$ equals zero $\mathbf{B}$ is positive definite.

A.3. Uncertainty-based global registration

First, it is proven that $\mathbf{B}$ is positive definite under the condition that the covariances $\mathbf{C}_{i,j}$ are positive definite. Second, the property of positive definiteness is shown for the covariances of both the Euler and quaternion representation.

Induction base $m = n$: Assuming a graph with $n + 1$ nodes and n links, the matrix $\mathbf{B}$ is transformed into a matrix $\mathbf{B}'$, by

$$\mathbf{B}' = \mathbf{I}_D \mathbf{B} \mathbf{I}_D^T,$$

with an upper-right triangular matrix $\mathbf{I}_D$ of six-dimensional identity matrices

$$\mathbf{I}_D = \begin{pmatrix} \mathbf{I}_{6\times6} & \cdots & \mathbf{I}_{6\times6} \\ & \ddots & \vdots \\ 0 & & \mathbf{I}_{6\times6} \end{pmatrix}$$

Since $\mathbf{B}'$ is given by

$$\mathbf{B}'_{j,j} = \mathbf{C}_{j-1,j}^{-1}$$
$$\mathbf{B}'_{j,k} = 0 \qquad (j \neq k)$$

and all covariances are positive definite, $\mathbf{B}'$ itself is positive definite. The same holds for $\mathbf{B}$, as $\mathbf{I}_D$ is invertible.

Inductive step $m \to m + 1$: Let $\mathbf{B}$ be a positive definite matrix that corresponds to a graph with $n + 1$ nodes and m links. An additional link between the nodes $\mathbf{X}_j$ and $\mathbf{X}_k$ is inserted, with the positive definite covariance $\mathbf{C}_{i,j}$. Without loss of generality, $\mathbf{X}_i$ is to be the fixed pose at 0. Thus, the resulting matrix $\mathbf{B}'$ is changed only at submatrix

$$\mathbf{B}'_{k,k} = \mathbf{B}_{k,k} + \mathbf{C}_{j,k}^{-1}.$$

$\mathbf{B}'$ is positive definite, iff

$$\mathbf{X}^T \mathbf{B}' \mathbf{X} > 0 \qquad \mathbf{X} \neq 0,$$

which is equivalent to

$$\sum_{m,l=1}^n \mathbf{X}_m^T \mathbf{B}'_{m,l} \mathbf{X}_l > 0 \qquad \mathbf{X}_m \neq 0. \tag{19}$$

Eq. (19) is expanded to

$$\sum_{m,l=1}^n \mathbf{X}_m^T \mathbf{B}'_{m,l} \mathbf{X}_l = \mathbf{X}_k^T \mathbf{B}'_{k,k} \mathbf{X}_k + \sum_{\substack{m,l=1 \\ m \neq k \neq l}}^n \mathbf{X}_m^T \mathbf{B}_{m,l} \mathbf{X}_l$$

$$= \mathbf{X}_k^T \mathbf{C}_{j,k}^{-1} \mathbf{X}_k + \sum_{m,l=1}^n \mathbf{X}_m^T \mathbf{B}_{m,l} \mathbf{X}_l = \mathbf{X}_k^T \mathbf{C}_{j,k}^{-1} \mathbf{X}_k + \mathbf{X}^T \mathbf{B} \mathbf{X} > 0.$$

$\mathbf{B}'$ is a positive definite matrix.

Euler angles: The covariance $\mathbf{C}_{j,k}$ is given by

$$\mathbf{C}_{j,k} = s^2 \mathbf{M}^T \mathbf{M}.$$

It can be safely assumed that $s^2 > 0$. Therefore, $\mathbf{C}_{j,k}$ is positive definite iff

$$\mathbf{X}^T \mathbf{M}^T \mathbf{M} \mathbf{X} > 0$$

or simply:

$$\sum_i \mathbf{M}_i \mathbf{X} \neq 0,$$

which is equivalent to:

$$\sum_i \begin{pmatrix} \theta_x \\ \theta_z \\ -\theta_y \end{pmatrix} \times \mathbf{m}_i \neq \begin{pmatrix} t_x \\ t_y \\ t_z \end{pmatrix}$$

for $\mathbf{X} \neq 0$. While this is not true iff all points $\mathbf{m}_i$ lie on two parallel lines, $\mathbf{C}_{j,k}$ is positive definite for all real data sets.

Quaternions: As above, $\mathbf{C}_{j,k}$ is positive definite iff:

$$\mathbf{X}^T \mathbf{M}^T \mathbf{M} \mathbf{X} > 0$$

or simply:

$$\sum_i \mathbf{M}_i \mathbf{X} \neq 0$$

which is equivalent to:

$$\sum_i p\mathbf{m}_i - \begin{pmatrix} q \\ r \\ s \end{pmatrix} \times \mathbf{m}_i \neq \begin{pmatrix} t_x \\ t_y \\ t_z \end{pmatrix}$$

for $\mathbf{X} \neq 0$. As above this is true for all real data sets.

Appendix B. Supplementary material

Supplementary data associated with this article can be found, in the online version, at doi:10.1016/j.cviu.2010.03.007.

References

[1] K.S. Arun, T.S. Huang, S.D. Blostein, Least square fitting of two 3-d point sets, IEEE Transactions on Pattern Analysis and Machine Intelligence 9 (5) (1987) 698–700.
[2] R. Benjemaa, F. Schmitt, Fast global registration of 3D sampled surfaces using a multi-Z-buffer technique, in: Proceedings of the IEEE International Conference on Recent Advances in 3D Digital Imaging and Modeling (3DIM '97), Ottawa, Canada, May 1997.
[3] R. Benjemaas, F. Schmitt, A solution for the registration of multiple 3D point sets using unit quaternions, Computer Vision – ECCV '98 2 (1998) 34–50.
[4] R. Bergevin, M. Soucy, H. Gagnon, D. Laurendeau, Towards a general multi-view registration technique, IEEE Transactions on Pattern Analysis and Machine Intelligence (PAMI) 18 (5) (1996) 540–547. May.
[5] P. Besl, N. McKay, A method for registration of 3-D shapes, IEEE Transactions on Pattern Analysis and Machine Intelligence 14 (2) (1992) 239–256.
[6] P. Biber, H. Andreasson, T. Duckett, A. Schilling, 3D modeling of indoor environments by a mobile robot with a laser scanner and panoramic camera, in: Proceedings of the IEEE/RSJ International Conference on Intelligent Robots and Systems (IROS '04), Sendai, Japan, September 2004.
[7] J. Böhm, S. Becker, Automatic marker-free registration of terrestrial laser scans using reflectance features, in: Proceedings of 8th Conference on Optical 3D Measurement Techniques, Zurich, Switzerland, July 2007, pp. 338–344.
[8] D. Borrmann, J. Elseberg, K. Lingemann, A. Nüchter, J. Hertzberg, Globally consistent 3d mapping with scan matching, Journal of Robotics and Autonomous Systems (JRAS) 56 (2) (2008) 130–142.
[9] D. Borrmann, J. Elseberg, K. Lingemann, A. Nüchter, J. Hertzberg, The efficient extension of globally consistent scan matching to 6 DOF, in: Proceedings of the Third International Symposium on 3D Data Processing, Visualization and Transmission (3DPVT '08), Atlanta, GA, USA, June 2008.
[10] Y. Chen, G. Medioni, Object modelling by registration of multiple range images, in: Proceedings of the IEEE Conference on Robotics and Automation (ICRA '91), Sacramento, CA, USA, April 1991, pp. 2724–2729.
[11] Y. Chen, G. Medioni, Object modelling by registration of multiple range images, Image and Vision Computing 10 (3) (1992) 145–155.
[12] S. Cunnington, A. Stoddart, N-View point set registration: a comparison, in: Proceedings of the 10th British Machine Vision Conference (BMVC '99), Nottingham, UK, 1999.
[13] T.A. Davis, Algorithm 849: a concise sparse Cholesky factorization package, ACM Transactions on Mathematical Software 31 (4) (2005).
[14] A.J. Davison, I. Reid, N. Molton, O. Stasse, Monoslam: real-time single camera slam, IEEE Transactions on Pattern Analysis and Machine Intelligence (PAMI) 29 (6) (2007) 1052–1067.
[15] M.W.M.G. Dissanayake, P. Newman, S. Clark, H.F. Durrant-Whyte, M. Csorba, A solution to the simultaneous localization and map building (SLAM) problem, IEEE Transactions on Robotics and Automation 17 (3) (2001) 229–241. June.
[16] U. Frese, Efficient 6-DOF SLAM with Treemap as a Generic Backend, in: Proceedings of the IEEE International Conference on Robotics and Automation (ICRA '07), Rome, Italy, April 2007, pp. 4814–4819.
[17] U. Frese, Efficient 6-DOF SLAM with Treemap as a Generic Backend, in: Proceedings of the IEEE International Conference on Robotics and Automation (ICRA '07), Rome, Italy, April 2007.
[18] U. Frese, G. Hirzinger, Simultaneous localization and mapping – a discussion, in: Proceedings of the IJCAI Workshop on Reasoning with Uncertainty in Robotics, Seattle, USA, August 2001, pp. 17–26.
[19] J.H. Friedman, J.L. Bentley, R.A. Finkel, An algorithm for finding best matches in logarithmic expected time, ACM Transaction on Mathematical Software 3 (3) (1977) 209–226. September.
[20] M. Greenspan, M. Yurick, Approximate K-D tree search for efficient ICP, in: Proceedings of the 4th IEEE International Conference on Recent Advances in 3D Digital Imaging and Modeling (3DIM '03), Banff, Canada, October 2003, pp. 442–448.
[21] G. Grisetti, S. Grzonka, C. Stachniss, P. Pfaff, W. Burgard, Efficient estimation of accurate maximum likelihood maps in 3d, in: Proceedings of the IEEE/RSJ International Conference on Intelligent Robots and Systems, 2007, pp. 3472–3478.
[22] C. Hertzberg, A framework for sparse, non-linear least squares problems on manifolds, Master's thesis, Universität Bremen, Bremen, Germany, November 2008.
[23] M. Hofer, Personal communication, 7 July 2008.
[24] M. Hofer, H. Pottmann, Orientierung von Laserscanner-Punktwolken, Vermessung & Geoinformation 91 (2003) 297–306.
[25] B.K.P. Horn, Closed-form solution of absolute orientation using unit quaternions, Journal of the Optical Society of America A 4 (4) (1987) 629–642.
[26] B.K.P. Horn, H.M. Hilden, S. Negahdaripour, Closed-form solution of absolute orientation using orthonormal matrices, Journal of the Optical Society of America A 5 (7) (1988) 1127–1135.
[27] S. Krishnan, P.Y. Lee, J.B. Moore, S. Venkatasubramanian, Global registration of multiple 3D point sets via optimization on a manifold, in: Eurographics Symposium on Geometry Processing, 2000.
[28] A. Lorusso, D. Eggert, R. Fisher, A comparison of four algorithms for estimating 3-D rigid transformations, in: Proceedings of the 4th British Machine Vision Conference (BMVC '95), Birmingham, England, September 1995, pp. 237–246.
[29] F. Lu, E. Milios, Globally consistent range scan alignment for environment mapping, Autonomous Robots 4 (1997) 333–349.
[30] M. Magnusson, T. Duckett, A comparison of 3D registration algorithms for autonomous underground mining vehicles, in: Proceedings of the Second European Conference on Mobile Robotics (ECMR '05), Ancona, Italy, September 2005, pp. 86–91.
[31] N.J. Mitra, N. Gelfand, H. Pottmann, L. Guibas, Registration of point cloud data from a geometric optimization perspective, in: R. Scopigno, D. Zorin (Eds.), Eurographics Symposium on Geometry Processing, 2004, pp. 23–32.
[32] A. Nüchter, K. Lingemann, J. Hertzberg, Cached k-d tree search for icp algorithms, in: Proceedings of the 6th IEEE International Conference on Recent Advances in 3D Digital Imaging and Modeling (3DIM '07), Montreal, Canada, August 2007, pp. 419–426.
[33] E. Olson, Robust and efficient robotic mapping, PhD thesis, Massachusetts Institute of Technology, Cambridge, MA, USA, June 2008.
[34] E. Olson, J. Leonard, S. Teller, Fast iterative alignment of pose graphs with poor initial estimates, in: Proceedings of the IEEE International Conference on Robotics and Automation (ICRA '06), 2006.
[35] L.M. Paz, J.D. Tardos, J. Neira, Divide and conquer: EKF SLAM in $O(n)$, IEEE Transactions on Robotics 24 (2008) 5.
[36] H. Pottmann, S. Leopoldseder, M. Hofer, Simultaneous registration of multiple views of a 3D object, ISPRS Archives 34 (3A) (2002) 265–270.
[37] H. Pottmann, S. Leopoldseder, M. Hofer, Registration without ICP, Computer Vision and Image Understanding (CVIU) 95 (1) (2005) 54–71.
[38] K. Pulli, Multiview registration for large data sets, in: Proceedings of the 2nd International Conference on 3D Digital Imaging and Modeling (3DIM '99), Ottawa, Canada, October 1999, pp. 160–168.
[39] S. Rusinkiewicz, M. Levoy, Efficient variants of the ICP algorithm, in: Proceedings of the Third International Conference on 3D Digital Imaging and Modelling (3DIM '01), Quebec City, Canada, May 2001, pp. 145–152.
[40] S. Schuhmacher, J. Böhm, Georeferencing of terrestrial laser scanner data for applications in architectural modeling, in: Proceedings 3D-ARCH 2005: Virtual Reconstruction and Visualization of Complex Architectures, vol. XXXVI, part 5/W17, 2005.
[41] A. Stoddart, A. Hilton, Registration of multiple point sets, in: Proceedings of the 13th IAPR International Conference on Pattern Recognition, Vienna, Austria, August 1996, pp. 40–44.
[42] S. Thrun, Robotic mapping: a survey, in: G. Lakemeyer, B. Nebel (Eds.), Exploring Artificial Intelligence in the New Millenium, Morgan Kaufman, 2002.
[43] S. Thrun, W. Burgard, D. Fox, A probabilistic approach to concurrent mapping and localization for mobile robots, Machine Learning and Autonomous Robots 31 (5) (1997) 1–25.
[44] S. Thrun, W. Burgard, D. Fox, Probabilistic Robotics, MIT Press, 2005.
[45] S. Thrun, D. Fox, W. Burgard, A real-time algorithm for mobile robot mapping with application to multi robot and 3D mapping, in: Proceedings of the IEEE International Conference on Robotics and Automation (ICRA '00), San Francisco, CA, USA, April 2000.
[46] B. Triggs, P. McLauchlan, R. Hartley, A. Fitzgibbon, Bundle adjustment – a modern synthesis, in: B. Triggs, A. Zisserman, R. Szeliski (Eds.), Vision Algorithms: Theory and Practice, in: Lecture Notes in Computer Science, vol. 1883, Springer-Verlag, 2000, pp. 298–372.
[47] M.W. Walker, L. Shao, R.A. Volz, Estimating 3-d location parameters using dual number quaternions, CVGIP: Image Understanding 54 (1991) 358–367.
[48] J. Williams, M. Bennamoun, Multiple View 3D Registration using Statistical Error Models, Vision Modeling and Visualization (1999).
[49] O. Wulf, A. Nüchter, J. Hertzberg, B. Wagner, Benchmarking urban six-degree-of-freedom simultaneous localization and mapping, Journal of Field Robotics (JFR) 25 (3) (2008) 148–163.
[50] Z. Zhang, Iterative point matching for registration of free-form curves, Technical Report RR-1658, INRIA-Sophia Antipolis, Valbonne Cedex, France, 1992.
[51] MESA Imaging, 2008. <http://www.mesa-imaging.ch/>.
[52] Robotic 3D Scan Repository, 2008. <http://www.kos.informatik.uni-osnabrueck.de/3Dscans/>.
[53] Zoller und Fröhlich Laserscanner, 2008. <http://www.zf-laser.com/>.
[54] ifm electronic, 2009. <O3D200 sensor, http://www.ifm.com/ifmuk/web/dsfs!O3D200.html>.
[55] PMDTechnologies GmbH, 2009. <http://www.pmdtec.com/>.